Pseudo-Shock Waves and Their Interactions in High-Speed Intakes

F. Gnani,* H. Zare-Behtash, and K. Kontis

University of Glasgow, School of Engineering, Glasgow G12 8QQ, UK

Abstract

In an air-breathing engine the flow deceleration from supersonic to subsonic conditions takes places inside the isolator through a gradual compression consisting of a series of shock waves. The wave system, referred to as a pseudo-shock wave or shock train, establishes the combustion chamber entrance conditions, and therefore influences the performance of the entire propulsion system. The characteristics of the pseudo-shock depend on a number of variables which make this flow phenomenon particularly challenging to be analysed. Difficulties in experimentally obtaining accurate flow quantities at high speeds and discrepancies of numerical approaches with measured data have been readily reported. Understanding the flow physics in the presence of the interaction of numerous shock waves with the boundary layer in internal flows is essential to developing methods and control strategies. To counteract the negative effects of shock wave/boundary layer interactions, which are responsible for the engine unstart process, multiple flow control methodologies have been proposed. Improved analytical models, advanced experimental methodologies and numerical simulations have allowed a more in-depth analysis of the flow physics. The present paper aims to bring together the main results, on the shock train structure and its associated phenomena inside isolators, studied using the aforementioned tools. Several promising flow control techniques that have more recently been applied to manipulate the shock wave/boundary layer interaction are also examined in this review.

* f.gnani.1@research.gla.ac.uk

CONTENTS

I. NOMENCLATURE

Roman Symbols

A	Cross-sectional area $[m^2]$
A/A_*	Isentropic area ratio dependent on the Mach number only
C_{f0}	Initial friction coefficient
C_P	Specific heat of air at constant pressure $[J/kgK]$
c	Coefficient of the velocity deceleration in high-speed pseudo-shock regions
D	Duct diameter $[m]$
D_θ	Degree of flow asymmetry
H	Duct height $[m]$
K_W	Airflow parameter
M	Mach number
P	Pressure $[Pa]$
P_0	Total pressure $[Pa]$
Re	Reynolds number
T	Temperature $[K]$
u	Freestream velocity $[m/s]$
w	Crocco number or dimensional velocity $[m/s]$
x	Generic position $[m]$

Greek Symbols

β	Experimental factor
γ	Ratio of specific heat capacity
δ	Boundary layer thickness $[mm]$
δ^*	Boundary layer displacement thickness $[mm]$
ζ	Correction factors for the mass flux
η	Correction factors for energy
θ	Boundary layer momentum thickness
μ	Mass flow ratio
ρ	Density $[kg/m^3]$

Subscript

0	Total condition
1	Initial condition
2	Exit condition
θ	Boundary layer momentum thickness

Superscripts

α	Reynolds number exponent
$*$	Sonic conditions
$'$	High-speed region
$''$	Low-speed region
$-$	Mass averaging quantity

II. INTRODUCTION

Human kind has been fascinated by flight and speed for centuries. The combination of these two concepts has inspired multiple generations of aerodynamicists and engineers to put great effort in developing high-speed aircraft since the first successes in flight history. The purpose of this paper is to carry out a review covering approximately one century of technological research on air-breathing propulsion, focusing on the engine intake and, in particular, on the role of the isolator and the associated flow structures which develop inside.

For high-speed vehicles travelling at high altitudes significant compression and heating of the air entering the combustion chamber are required. The principle, which characterises the so-called air-breathing engine such as ramjet and scramjets (supersonic combustion ramjets), takes advantage of the high-speed airflow physics and compresses the air by means of internal geometry changes. This approach allows the engine to operate beyond the flight speeds at which the gas-turbine engine becomes inefficient and has become particularly attractive due to its simplicity for the absence of moving components.

The mechanism of flow compression, which takes place in a ramjet or scramjet inlet, finds other relevant applications characterised by the interaction of shock waves with the boundary layer such as supersonic compressors, ejectors, and wind-tunnel diffusers.[1] Therefore, the ability to accurately predict and control shock wave structures would provide a means to enhance the performance of flow devices operating at high speeds, the engine efficiency, or the mixing of fuel injected from the combustor walls.[2]

The origins of ramjet technology were laid down around a century ago, in 1913, when a French engineer, René Lorin, published an article in the aviation magazine *L'Aérophile* expressing the idea to create jet propulsion by directing the exhaust gases from internal combustion engines into nozzles.[3] However, due to the lack of materials and technological limitations of the time, he could not have advanced this concept beyond the design stage.[4]

Ramjet technology gained maturity after World War II. In 1947 the world's first aircraft powered exclusively by a ramjet, *Leduc 0.10*, illustrated in Figure 1, successfully performed the first powered flight.[6] Since it could not take off unassisted, the aircraft needed to be carried and then released by a mothership at the appropriate altitude. In a subsequent flight, in 1949, the *Leduc 0.10* was released by a *Languedoc S.O.161* at 36,000 ft achieving the necessary pressure conditions for the ramjet to sustain power.[7] Nine years later, in 1958,

the *Nord 1500 Griffon*, shown in Figure 2, reached Mach 2.19, marking the first significant success in ramjet technology. A step further was made by Antonio Ferri,[8] who revolutionised the design of high-speed vehicles proposing a new type of supersonic inlet, as illustrated in Figure 3, in which all the parts intended for the deceleration of the supersonic flow were placed outside of the diffuser. It was then recognised that an air-breathing propulsion vehicle could fulfil the possibility of hypersonic cruise and recoverable space launchers, a feature not achievable with rocket engines.[9]

For Mach numbers greater than 3, but below approximately 5, several configurations of air-breathing engines have been proposed depending on the mission requirements in order to provide sufficient mass flow, adequate lift and propulsion. In this flight regime the pure ramjet, illustrated in Figure 4,[10] provides the most efficient thermodynamic cycle.[11] The flow is choked at the inlet, downstream of the isolator, causing a large back-pressure at the combustor entrance and the formation of a sequence of shock waves inside the isolator which guarantees that the air enters the combustor at subsonic speeds ($M \sim 0.3 - 0.4$).[12] The isolator is a nearly parallel duct placed between the inlet and the combustor with the purpose of containing the shock wave structures and preventing the interaction of the flow at the inlet with that inside the combustion chamber.[13] The presence of this component has been found effective in increasing the combustion heat release,[14] and higher engine thrust can be achieved if the precombustion shock is confined to the isolator.[15]

As the flight Mach number increases above 5, the deceleration of air to subsonic conditions introduces two problems. Firstly, the pressure rise to decelerate the flow to subsonic speed drastically increases the pressure losses associated with shock waves. The second issue is the increased gas temperature to very high values in the combustor.[16] This effect is not only responsible for structural problems, requiring an adequate selection of the wall material and cooling methods in the combustor, but also provokes chemical dissociation so that the combustion products might not be completely formed with consequent penalties in the engine cycle performance.[17]

At flight speeds above Mach 8, the kinetic energy of the flow through the engine becomes high enough that the combustion pressure rise does not cause boundary layer separation. The flow is gradually decelerated at the inlet to a lower speed but remains supersonic in the combustor, where the fuel is injected and mixed with the flow. This configuration, called a pure scramjet, is illustrated in Figure 5. When the engine operates in scramjet mode, there is

no shock train since the flow is supersonic through the entire engine and the isolator appears to be unnecessary. However, the area increase in the combustor is often not sufficient to mitigate the thermal choking caused by heat addition which enhances the adverse pressure gradient, favouring the unstart of the engine.[11] If a sudden pressure increase takes place, the wall boundary layer separates and the pressure rise propagates upstream. In this case the presence of the isolator helps to ensure that, even though the boundary layer is separated over a large portion of the duct, the core flow remains supersonic and forms an oblique shock train that contains the phenomenon of engine unstart.

The unstart of a hypersonic inlet is a phenomenon in which the shock wave structure developed inside the inlet is expelled outside, producing an abrupt reduction in the captured mass flow and total pressure due to the spillage of air. This causes a significant drop of engine thrust and specific impulse. As reported by Wagner et al.,[18,19] the unstart flow structure is highly three-dimensional and, since this phenomenon is remarkably violent and may cause catastrophic damages to the aircraft during flight, it must be avoided and controlled.[20]

The isolator plays a significant role on the flow transition from supersonic to subsonic conditions in dual-mode scramjet combustors.[21] Dual-mode ram-scramjets (DMR) or dual-combustor ramjets (DCR), illustrated in Figure 6, were introduced during the 1970s by the Applied Physics Laboratory (APL) and allow the engine to operate at both low and high supersonic Mach numbers,[15] i.e. as a ramjet with high Mach number but subsonic combustion or as a scramjet with supersonic combustion. At dual-mode conditions, the fuel is injected at either sonic or supersonic conditions and the combustion process occurs at subsonic conditions in a constant area duct which then becomes divergent. In this configuration the core flow is decelerated to subsonic conditions by the combined effect of the injection and heat release upstream of the fuel injector ports generating a shock train that extends into the combustion chamber.[22]

For Mach numbers from 8 to 18, the scramjet exhibits good performance. However, above Mach 18, friction losses increase considerably and scramjet operation becomes difficult. The performance gradually decreases approaching that of the rocket engine.[12] The amount of available energy due to combustion is also a much smaller fraction of the incoming kinetic energy, which leads to little gains to be had.

III. PSEUDO-SHOCK WAVES

During flight, the low density air enters the engine inlet, where it is compressed before reaching the combustor. In the majority of high-speed inlets the flow compression is performed with both external and internal processes by means of shock waves. Internal compression is achieved inside the isolator through an extremely complex mechanism characterised by a shock wave structure that spreads over a long distance in the flow passage.[13] The fuel combustion causes a rapid pressure rise in the combustion chamber and the formation of a shock structure inside the isolator results in different conditions upstream and downstream of the flow passage.

Crocco[23] pointed out that the deceleration from supersonic to subsonic velocity does not occur through a normal shock, but with a more complicated and gradual transition, also confirmed by Matsuo et al.[24] In the inviscid limit, in the absence of a boundary layer, the shock structure would be a single normal shock wave.[25] However, due to the existence of a viscous boundary layer, this simple pattern rarely occurs and the shock structure is spread into a series of oblique or lambda shock waves.[10]

The fundamental characteristics of the interaction between a shock wave and the boundary layer with the creation of a series of shocks was initially described by Crocco.[23] The shock wave/boundary layer interaction creates a local thickening of the boundary layer and leads to the formation of a virtual nozzle throat. As illustrated in Figure 7, a throat-like geometry generates between two consequent shocks with a resulting change in the duct cross-section. Therefore, immediately downstream of the main shock, the flow is accelerated again to supersonic speeds through this virtual nozzle until the next shock recompresses the flow again.[26,27]

The pseudo-shock system depends on the passage geometry, wall friction, Mach number, Reynolds number based on the tube height, boundary layer thickness, and pressure conditions at the two extremities of the duct.[11] As the flow Mach number increases, the effect of increased blockage becomes more relevant with consequent promotion of multiple shock interactions, production of lower pressure recovery, and extension of the wave structure along the duct.[28] Lustwerk[29] observed that the shock wave structure changes depending on the variation of the boundary layer thickness upstream of the shock train, also referred to as flow confinement.[24] The flow confinement is defined as the ratio of the undisturbed

boundary layer thickness, δ, to the duct half height, H. This is in agreement with Babinsky & Harvey,[30] who reported that multiple shocks are more likely when the ratio of boundary layer displacement thickness to duct height is greater than a few percent. Weiss et al.[31] confirmed that the confinement level and Mach number are the dominant variables which characterise the position and length of the shock train, whereas the Reynolds number has a much smaller effect, and therefore different experiments can be easily compared.[32] On the other hand, it was reported by Neumann and Lustwerk[33] that the length of the shock region is affected by scale effects since it depends on the equivalent length-diameter ratio. Fischer & Olivier[34] have more recently demonstrated that the shock train length is dependent on the ratio of the wall temperature to that of the free stream flow. Adiabatic or hot-wall boundary layers are less resistant to adverse pressure gradients than cold-wall boundary layers because cold-wall boundary layers are thinner and have higher skin friction.

A. Pseudo-Shock Structure

As illustrated in Figure 8(a), with shock Mach numbers up to 1.2, a very weak interaction takes place: the shock wave is close to an inviscid normal shock and no separation occurs at the wall.[24] Ikui et al.[35] reported that with a low Mach number the shock wave/boundary layer interaction is weak (see Figure 8(b)). The shock is nearly normal and changes inclination continuously with increasing distance from the wall;[36] the boundary layer is thin with possible separation, which however tends to reattach immediately. As the Mach number increases up to approximately 1.5, as in Figure 8(c), a stronger interaction takes place and the foot of the shock bifurcates near the wall surface, gradually forming a λ shape. The boundary layer at the shock becomes thicker and the pressure rise of the shock is sufficient to generate locally separated regions. Over Mach 1.5 the compression downstream of the shock becomes stronger and forms successive shock waves with regular or Mach-type reflections,[37] in Figure 8(d). At a Mach number of 1.86, the λ shape changes into a χ shape, and at a Mach number of 2.42, the shock structure transitions to one defined by a series of weak oblique shocks. Sugiyama et al.[38] observed the λ-shape structure up to Mach 2, but at a Mach number of 4 a dramatic change of the separation mechanism takes place, in agreement with Hataue,[39] who faced some difficulties in observing a clear pseudo-shock at Mach 3. Sullins[10] was able to observe the formation of the precombustion shock system at

a Mach number of 5.7, but above Mach 5.95 the pressure in the combustor reaches a value below the separation pressure and the shock system is eliminated as the combustion process transitions to pure scram-mode. The flow remains supersonic through the entire engine and the isolator is used as a constant area combustor with fuel injectors installed upstream of the isolator, as illustrated in Figure 9.

Figure 10 shows the two typical configurations experimentally observed as the conditions at the end of the shock train change, the λ-shock in Figure 10(a) and the χ shape in Figure 10(b). The approximate Mach number at which this distinction takes place is in the range between 2 and 3.[41] The series of normal shock waves, characteristic of flows with thick inlet boundary layers and low Mach numbers, in Figure 11(a), is composed of successively decreasing strength and distance between succeeding shocks up to the point where a terminal shock occurs.[26] The major portion of the compression takes place at the first normal shock which splits into two different parts as it interacts with the wall separating the boundary layer, namely a normal shock in the centre of the duct, and oblique shock waves near the wall. After the first shock, the boundary layer reattaches and grows rapidly, and a series of small secondary normal shocks develop, resulting in a dissipative process of sequential decelerations and accelerations of the flow.[15] With higher Mach numbers and in the presence of a larger flow confinement, the first shock becomes oblique. Carroll et al.[42] observed that the same behaviour extends also to the subsequent shock waves, and the flow pattern, called oblique shock train, is similar to that depicted in Figure 11(b). In this case, the initial oblique shock separates the boundary layer, reflects from the opposite walls of the duct, and propagates downstream alternating between compression and expansion. The boundary layer remains separated for long distances.

When the interaction of the shock wave with the boundary layer is particularly strong, the shock train is followed by a mixing region, after which the flow is fully subsonic and uniform. The entire structure, schematically shown in Figure 12, is called a pseudo-shock wave.[35] According to Ostras and Penzin,[43] the pseudo-shock is composed of a dissipation layer at the walls, and a central almost isentropic layer. The mixing region, called supersonic tongue by Om et al.,[28] consists of a double-tongue-shaped supersonic flow, which passes through a system of compression waves near the centreline of the duct, bounded by a subsonic outer region.[31] This region changes its shape and extension with Mach number due to the boundary layer thickening and its occurrence depends on the duct length.[24,42] Radial, axial

and circumferential gradients of the flow properties and chemical composition in the mixing region have been hypothesised and confirmed. Nagai[44] observed that the radial distribution of the total and static pressure across the shock train is subject to complicated changes due to the presence of shock waves and viscous diffusion, as illustrated in Figure 13. Nevertheless, some discrepancies with the computed prediction of the mixing region are present since, compared to experimental observations, a smaller embedded supersonic region behind the shock has been obtained.[28]

A typical pressure variation through a pseudo-shock is illustrated in Figure 14. In the initial portion of the shock train, the pressure increases rapidly because of the oblique or bifurcated normal shock waves. At the centre of the duct the flow undergoes successive local changes from supersonic to subsonic by multiple normal shocks, which are not detected by wall pressure measurements because the surface pressures tend to be smeared out due to the dissipative behaviour of the boundary layer. In the mixing region, for $X = 5$ to 11 in Figure 14, the pressure continues to rise with a lower rate until it reaches a maximum where the flow is decelerated to subsonic speeds, after which the flow is accelerated again, and the pseudo-shock region terminates.[24] The actual separation of the shock train and the mixing region is not clearly defined because pressure measurements are not able to significantly show changes between the two regions.[31] It can be observed that the pressure increases rapidly through the shock train and more moderately in the mixing region: 50% of the maximum pressure rise is achieved in approximately 1/4 of the shock length, and 80% in approximately 1/2.

For each Mach number, the pressure recovery along the shock train is smaller compared to that through an inviscid normal shock wave since each shock causes a significant total pressure loss[37] and viscous effects in the mixing region.[31] The static pressure ratio across the shock train reduces as the boundary layer displacement thickness increases, and this trend becomes more evident for higher Mach numbers.[45] As the experimental data in Figure 15 show, the maximum isolator exit pressure is achieved when the pseudo-shock and the isolator are of the same length. The length of the pseudo-shock is defined as the region from the head of the shock train to the end of the subsequent static pressure recovery region. It increases with both the boundary layer thickness relative to the duct diameter and the Mach number upstream of the shock train, and has been found to vary in the range of 4 to 15 tube diameters.[46] Therefore, the isolator must be designed to be of sufficient length

to prevent inlet unstart, but not overly long to avoid excessive weight and additional shear losses.[15] As Reinartz et al.[47] experimentally observed, the growth of the boundary layer introduces viscous losses which cancel out the advantage of an additional length. On the other hand, the magnitude of the pressure profile decreases with decreasing isolator length, and this trend becomes more evident for higher Mach numbers.[48,49]

The optimum length of a constant area passage has been found to lie between 8 to 12 tube diameters for Mach numbers from 1.8 to 4.2.[33] According to Sullins,[13] with a duct length of 10 to 20 duct heights, the shock train pressure rise can reach up to 95% of the normal shock strength but, as pointed out by Emami et al.,[50] the optimal isolator length must be designed as a trade-off of all the component requirements over the flight envelope.

B. Pseudo-Shock Oscillations

The description of the pseudo-shock wave mechanism is further complicated by the presence of a violent and irregular oscillating behaviour, which was initially investigated by Ikui et al.[51] and confirmed by further studies.[52–54] High-speed schlieren, obtained by Gawehn et al.[27] and illustrated in Figure 16, shows that each shock wave of the shock train is not located at a fixed point but oscillates with time about its time-mean position even when the upstream and downstream pressures remain constant. Yamauchi et al.[55] encountered some difficulties in visualising the pseudo-shock wave in the PIV mean streamwise velocity because of the intense shock wave fluctuations.

Experimental data from Ikui et al.[51] showed that the oscillation amplitude of the first shock of the shock train is smaller than those of the subsequent shock waves, leading the authors to the conclusion that the oscillation of the first shock influences the oscillation of the entire flow structure. The mechanism of the pseudo-shock oscillation was described by Yamane et al.[56,57] to be caused by the interaction of two frequencies which travel in the opposite direction and excite each other. The pressure fluctuation due to the oscillation of the air in the divergent passage downstream of a straight duct travels upstream through the pseudo-shock and excites the first shock oscillation. This generates a strong pressure fluctuation which propagates downstream and, in turns, maintains the oscillation in the channel.

Gawehn et al.[27] hypothesised that the axial movement of the pseudo-shock oscillation is

caused by the boundary layer oscillations in the pseudo-shock region. Sugiyama[58] conjectured the oscillation mechanism of the pseudo-shock wave to be caused by the thickening of the boundary layer in proximity of the first shock wave of the shock train. A throat-like shape generates between the first and the second shocks changing the actual throat cross-section. Since the boundary layer thickness changes along the duct, the throat cross-section also changes and induces the first shock to oscillate with a frequency that depends on the basic oscillation of the air column between the first shock and the duct exit. Similarly, the computed results in the core flow obtained by Robinet & Casalis[59] showed an increase of the longitudinal mean velocity behind the shock due to the expansion caused by the separation bubble in the boundary layer. The authors however demonstrated that the self-sustained oscillation can be predicted with the inviscid quasi-one-dimensional stability theory and, therefore, this phenomenon is not caused by the transverse waves carried by the boundary layer.

According to Sajben et al.,[36] the characteristics of the fluctuations are dependent on the cause of separation, i.e. pressure-gradient or shock-induced separated flows. Su & Zhang[60] identified the backpressure as an important variable on the shock train unsteadiness. Hsieh & Coakley[61] found the oscillation frequency dependent on the duct length-to-height ratio. Bogar et al.[62,63] observed downstream-travelling counter-rotating vortices originating near the upstream edge of the separation bubble, but no information has been deduced to relate the vortices characteristics with the oscillation frequency.

Gawehn et al.[27] also observed that, while oscillating, the shock structure changes between symmetric and asymmetric, but this behaviour was not captured by numerical simulation even using the unsteady three-dimensional Navier–Stokes equations. Similar results were obtained by Sun et al.[40] who observed the shock system randomly attached to the bottom or top wall in the experiments, but the computations were not able to reproduce the asymmetric characteristics. Xiao et al.[64] observed that, for a supersonic flow in a convergent-divergent nozzle with a moderate expansion ratio, the flow asymmetry does not switch sides during a given run. However, for the same level of perturbation, from one experimental run to another, the asymmetry could change side, in agreement with Papamoschou et al.[65,66] The numerical investigation in diverging isolators with rectangular cross-section by Kawatsu et al.[67] led to the finding that a large separation region appeared at only one corner of the test section. Additionally, once the separation is formed, it remains in the same position and

does not move to another corner. This asymmetry generates a violent noise and fluctuating wall load which, if strong enough, may provoke fatigue failure.[24]

In contrast to attached flows, the acoustic characteristics in the presence of flow separation has been found to be more complicated and not predictable with the acoustic theory.[62] Hsieh et al.[68] imposed a sinusoidal pressure fluctuation at the exit plane of the diffuser to simulate the response of a ramjet inlet to the unsteadiness of the combustion chamber using two-dimensional Navier–Stokes equations. The computed solution showed a non-sinusoidal variation of velocity at the exit plane, in contrast with both the acoustic theory and small-perturbation models, which predict a sinusoidal velocity variation of the same frequency with altered phase angle and amplitude.

A recent investigation by Oh et al.[69] reproduced the movement of the terminal shock in response of an externally imposed pressure oscillation in the diffuser. This produced large vorticity fluctuations in the radial direction, as well as variations of the size of the boundary layer separation and the terminal shock configuration. The authors concluded that a supersonic inlet under supercritical operation acts as an effective acoustic damper absorbing disturbances arising downstream. Cohen and Valerino[70] demonstrated that the application of boundary layer suction upstream of the normal shock present in a duct of constant area cross-section is effective in reducing the oscillation amplitude. However, the knowledge of the oscillation phenomenon in pseudo-shocks is still not completely understood and further investigations are required.

C. Isolator Duct Geometry

The pseudo-shock structure is significantly affected by the area change, because it extends over a great distance along the passage, and even in a straight channel the analytical calculation of the pseudo-shock length is very complicated.[71] However, the numerical computation of a pseudo-shock length in a slightly divergent duct is easier than the constant area case since geometry plays a role in the stabilization of the shock system. For a constant area duct the only thing keeping pseudo-shock length fixed is the deformation of the boundary layer due to the interactions with the shock wave.

Small divergence or constant area ducts produce higher efficiencies of shock compression because, in this condition, there exists a positive velocity gradient in the subsonic flow

downstream of the shock compression region which stabilises the boundary layer and reduces separation.[29,72] According to Walther et al.[73] the use of divergence angles of 1°–2° on both the duct walls of the combustor inlet is effective in mitigating the steep static pressure rise downstream of the fuel supply point and counteracts the thermal blockage by heat addition. The small level of divergence is meant to counteract the boundary layer growth so that the effective fluidic cross-section remains constant. Huang et al.[21] found that small divergence angles of the isolator due, for example, to the manufacturing process, may have a significant impact on the shock structure in scramjet isolators. Figure 17 shows the effect of the divergent angle on the shock train with a constant value of the back pressure. As the divergence angle increases from 0° to 1.0^o, the front of the shock wave moves towards the entrance of the duct, and the shock train changes from the oblique to the normal shock configuration. However, for duct angles greater than 1.5^o, the flow expansion at the entrance of the isolator generates a more serious boundary layer separation on the walls. The front of the shock train is pushed downstream with a zone of negative pressure ahead of the shock train and the shock train exhibits again the oblique shock characteristics. This is due to the fact that small expansion angles can reduce the effect of the boundary layer separation and decrease the intensity of the first shock wave. When the expansion angle is increased enough the boundary layer separation becomes so strong that it cannot be counteracted by the beneficial effect of the expansion angle. This behaviour is illustrated in Figure 18.

The majority of research on high-speed isolators has focused on cylindrical ducts, and only recently on rectangular cross-sections. This choice is due to the fact that the axisymmetric configuration minimises the three-dimensional effects from the shock wave/boundary layer interactions which have been found in rectangular channels.[26] Kawatsu et al.[67] reported that in diverging rectangular ducts a large separation of the boundary layer caused by the first shock of the shock train occurs only at one corner of the upper wall of the test section (Figure 19), whereas in the constant area duct case the separated region was observed near all the corners of the duct. Additionally, in the constant area duct, from both numerical and experimental results shown in Figure 20, the boundary layer separation occurs only near the corners of the duct but not at the centre plane of the test section as it might by though by schlieren photography. The circular duct has the strongest capability for supporting the combustion backpressure compared with other shapes.[74]

Billig et al.[15] stated that the trend of the pressure rise for cylindrical and rectangular

cross-sections is quite similar, suggesting that the shock train characteristics may also be similar. As reported by Bement et al.[14] no similarity law linking the various geometries and the applicability of correlations to the design of rectangular isolators have yet been established. Lin et al.[74] showed that, compared to rounded cross-sectional area ducts, in the rectangular configuration the pressure profile of the shock train initially rises steeply, reaches a maximum value early, and drops quickly at the isolator exit. Also, the maximum pressure rise is smaller, independent of the Mach number. These differences were attributed to the fact that in the rectangular duct, the larger cross-sectional perimeter and the presence of the four corners both lead to an increased cross-sectional area of the duct covered by the boundary layer, thus reducing the effective free-stream area. On the other hand, for the same Mach number, the leading edge of the shock train was detected to be roughly at the same axial position inside the isolator for both circular and rectangular cross-sections. Sridhar et al.[75] numerically obtained almost the same total pressure recovery for isolators of square and square-to-circular shapes. However, as illustrated in Figure 21, the two geometries led to different flow characteristics, i.e. the square isolator is characterised by a longer shock structure with the shock train front placed more upstream, and thinner and longer separated regions due to the influence of corner vortices.

The macroscopic structures and characteristics the shock train forms in rectangular ducts have mostly been investigated for Mach numbers up to M=2. Few studies have covered higher Mach numbers and Sugiyama[38] was one of the first to extend the range up to M=4. Sullins[13] noticed that the back pressure can be controlled without moving the shock train, using a step in the duct as schematically illustrated in Figure 22. When the shock train starts downstream of the step, the maximum pressure is less than that in a constant area duct and a significantly longer duct is required to reach the same pressure. When the shock train starts upstream of the step, the area expansion caused by the step yields a slightly higher pressure due to subsonic diffusion across the step.

It is worth mentioning that a pseudo-shock wave also forms downstream of a De Laval nozzle exit with an over-expanded jet. Nagai[44] experimentally observed that the normal shock changes into a pseudo-shock wave immediately after its occurrence in the flow with the static pressure undergoing strong overcompressions and overexpansions until it achieves the back-pressure. Furthermore, the pseudo-shock wave which establishes downstream of the nozzle is characterised by asymmetry respect to the jet axis. This asymmetry is highlighted

by the presence of sound waves propagating in all directions and is likely due to asymmetries present in the geometry of the nozzle. A schlieren image of this phenomenon is illustrated in Figure 23.

IV. ANALYTICAL AND NUMERICAL MODELLING OF PSEUDO-SHOCK SYSTEMS

An extensive investigation on pseudo-shock waves was carried out by Matsuo et al. in 1999[24] and other experimental studies with the aim of validating the various analytical models used.[31] The numerous variables which contribute to generating a complicated interaction between the shocks and the boundary layer make the comprehensive analysis of the flow field extremely challenging. For this reason, simplified analytical formulations have been developed to estimate the pressure distribution and the length required to achieve the necessary pressure rise in the isolator. The advantage of this conservative approach is that it allows the parametrisation of the static pressure using only the conditions ahead of the shock train as well as avoiding the solving of the full Navier–Stokes equations.[76] The majority of the models assume the absence of heat transfer, however if surface heat transfer is included, the local and global effects of a shock wave/boundary layer interaction will be altered.[77] As stated by Inger et al.,[78] even a small variation of the surface temperature above the adiabatic value significantly influences the global aerodynamics and therefore the solution of the governing equations.

The flow in pseudo-shock waves is far from being one-dimensional,[24,27] but the coarse mechanism of formation of multiple shock waves can be explained through an equivalent one-dimensional model, as outlined by Om and Childs[26] and shown in Figure 24. The first shock wave causes an increase of the boundary layer thickness large enough to choke the flow. Therefore, the subsonic flow immediately behind the first shock wave is accelerated through the converging channel between section AA and BB, where it reaches sonic conditions. After section BB, the divergent duct induces the supersonic flow to expand and form a second normal shock wave. At this point, the increased thickness of the boundary layer starts the same process described for the first normal shock. The second normal shock in turn produces another normal shock wave, and the mechanism is reproduced until the normal shock wave becomes weak enough that the flow is not choked any more.

The theoretical total pressure recovery through a normal shock in a duct having an initial boundary layer was initially calculated by McLafferty[1] with Equation 1 on the basis of continuity, conservation of momentum, and conservation of energy,

$$\frac{P_{02}}{P_{01}} = \left(\frac{P_1}{P_{01}}\right)\left(\frac{P_{02}}{P_2}\right)\frac{K_{W1}}{K_{W2}}\left(1 - \frac{2\delta^*}{H}\right) \tag{1}$$

where K_W is a airflow parameter defined as:

$$K_W = \frac{2}{H}\int_0^{H/2} \frac{1}{(P/P_0)\,(A/A_*)} dy \tag{2}$$

With the assumptions of the formation of a normal shock wave and negligible viscous effects, the calculated total pressure recovery through a normal shock is reduced by an amount proportional to the displacement thickness of the boundary layer approaching the shock. In reality, shock compression in divergent ducts exhibits a gradual increase in pressure at the wall, confirmed by the pressure measurements obtained by Castagna.[79] Although this discrepancy illustrated the inadequacy of the normal shock theory, the accuracy was found to increase with smaller duct divergence angles and higher Mach numbers.

Crocco[23] and Tamaki et al.[80,81] proposed two analytical models assuming the overall pressure ratio across the shock train equals that of a normal shock and neglecting the effect of the upstream boundary layer and wall friction in the pseudo-shock region. With its simplicity, the Crocco's *shockless model*, schematically illustrated in Figure 25 and expressed by Equation 3, reveals the essential characteristics of the pseudo-shock,

$$\frac{P}{P_1} = \left(\frac{1 - w'^2}{1 - {w_1}^2}\right)^{\frac{\gamma}{\gamma-1}} \tag{3}$$

where w is the Crocco number or non-dimensional velocity defined as:

$$w = \frac{u}{\sqrt{2C_P T_0}} \tag{4}$$

The model developed by Tamaki et al.[80,81] referred to as the *shock reflection model*, states that not only the wall but also the main flow is affected by pressure changes. The description of the variation of static pressure occurs across successive oblique shock waves and, therefore, the shock angles of the series of shock waves in the shock train are needed in advance. Even

though the mathematical formulation was different, the results of both the models led to the same flow properties, which significantly diverged from the experimental data.

The assumptions which the *shockless model* relies on have been found to be the source of the discrepancy with experimental investigations and an improved model, called the *diffusion model*, was proposed by Ikui et al.[35] The model is illustrated in Figure 26 and the analytical form is defined by Equation 5,

$$\frac{P - P_1}{P_2 - P_1} = \frac{\left[{w_1}^2 \left({w_1}^2 - 2{w^*}^2\right) + {w_1}^2 {w^*}^2 E\right](1 - E)}{\left({w_1}^2 - {w^*}^2\right)^2 - {w_1}^2 \left({w_1}^2 - {w^*}^2\right) E\,(1 - E)} \tag{5}$$

where $E = e^{-c(x/D)}$, w^* is the Crocco number at sonic conditions, and c a coefficient experimentally determined for the deceleration of velocity in high-speed regions of the pseudo-shock:

$$\frac{dw'}{dx} = -cw' \tag{6}$$

This model removes the assumption of the Crocco's *shockless model* of isentropic flow in the centre of the duct and it is able to determine the length of the shock train, defined as the distance where the velocity in the central core region becomes equal to that in the outer dissipative region. In spite of the closer agreement with experimental data, discrepancies remained particularly for low Mach numbers due to the fact that a low supersonic flow is not fully diffused within the distance, leading to a significant deviation from the assumptions of the uniform flows both upstream and downstream of the pseudo-shock.

More accurate agreement with empirical data was obtained with further improvements by Ikui et al.[46] if the effect of the upstream boundary layer and wall friction losses is included in the model schematically illustrated in Figure 27 and defined by Equation 7,

$$\frac{P}{P_1} = \frac{1}{\xi}\left[\frac{(1-\mu)}{M'}\left(1 + \frac{\gamma - 1}{2}M'^2\right)^{-1/2} + \frac{\mu}{M''}\left(1 + \frac{\gamma - 1}{2}M''^2\right)^{-1/2}\right] \tag{7}$$

where μ denotes the mass flow ratio m''/m and ξ is defined as follows:

$$\xi = \frac{(1-\mu_1)}{M_1'}\left(1 + \frac{\gamma - 1}{2}M_1'^2\right)^{-1/2} + \frac{\mu}{M_1''}\left(1 + \frac{\gamma - 1}{2}M_1''^2\right)^{-1/2} \tag{8}$$

All the aforementioned models have the limitation that only the pressure rise through the shock train region can be determined. An empirical quadratic correlation method for

cylindrical ducts, expressed by Equation 9, was proposed in the 1970s by Waltrup et al.[82–84] to relate the distance over which the shock structure is spread with the flow parameters,

$$\frac{x\left({M_1}^2-1\right){Re_\theta}^\alpha}{D^{1/2}{\theta_1}^{1/2}}=50\left(\frac{P}{P_1}-1\right)+170\left(\frac{P}{P_1}-1\right)^2 \tag{9}$$

where D is duct diameter, M_1 the Mach number, θ_1 the boundary layer momentum thickness, Re_θ the Reynolds number based on the boundary layer momentum thickness, and P/P_1 the pressure rise across the shock train. This equation requires the determination of the boundary layer momentum thickness along the isolator wall, which depends on the surface roughness, flow conditions, and the Mach number upstream of the shock train. This method was corrected by Billig[85] for its applicability to rectangular ducts by substituting the duct diameter D with the duct height H, as Equation 10 illustrates,

$$\frac{x\left({M_1}^2-1\right){Re_\theta}^\alpha}{H^{1/2}{\theta_1}^{1/2}}=50\left(\frac{P}{P_1}-1\right)+170\left(\frac{P}{P_1}-1\right)^2 \tag{10}$$

Weiss et al.[31] analysed the different shock train models with different pressure levels and Mach numbers up to M=2.0. They concluded that the model developed by Billig[85] in Equation 10 most accurately reproduced the pressure gradient for the shock train in a rectangular duct at low Mach numbers, in particular in the shock train region. However, a better agreement between the measured and predicted values of the shock train length in the Mach number range from 1.33 to 1.85 was obtained by Wang et al.[86] with an additional correction including the degree of flow asymmetry, D_θ:

$$\frac{x\left({M_1}^2-1\right){Re_\theta}^\alpha}{(1+D_\theta)^\beta H^{1/2}{\theta_1}^{1/2}}=50\left(\frac{P}{P_1}-1\right)+170\left(\frac{P}{P_1}-1\right)^2 \tag{11}$$

where the factor β assumes values based on the actual measured data. The parameter D_θ is defined as:

$$D_\theta=\frac{\theta_{max}-\theta_{min}}{\theta_{max}}\times 100 \tag{12}$$

with θ_{max} and θ_{min} defined as the boundary layer momentum thickness corresponding to different values of boundary layer thickness at the two walls of the duct, as Figure 28 illustrates.

It can be observed that when D_θ is zero the flow is completely symmetric at the isolator entrance and Equation 11 reduces to Equation 10. This experimental correlation was

introduced because, in reality, the flow field inside the isolator is asymmetric, even though researchers have put a great deal of effort in studying symmetric conditions.[86] It was also observed that, for a given pressure ratio, the length of the shock train becomes larger as the asymmetry of the flow grows.

Additionally, in Equations 9 to 11, the Reynolds number exponent α assumes the value of 1/4 obtained from a regression analysis of the data.[85] However, a recent paper by Sridhar et al.[75] achieved $\alpha = 0.225$ by averaging the values of square and circular ducts.

Zimont and Ostras[87] studied the pseudo-shock in presence of a fairly thick boundary layer and formulated the *jet-flow model* assuming a supersonic jet-like nature of the dissipation zone development. Although the static pressure rise agreed well with experimental results, the model is quite complex due to the presence of the Bessel function in the integral equations.

If the Mach number and the static pressure inside the pseudo-shock are known, the *separation model* proposed by Shchetinkov[88] approximately predicts the configuration of the separation region. The model assumes a negligible flow velocity in the separation region, the transverse pressure gradient at any cross-section and the variation of total temperature through the pseudo-shock region.

Neglecting the wall friction and heat transfer inside the pseudo-shock, Nagai and Yaga[89] formulated a relationship through Equation 13, in which the ratio of the total pressure at the final and initial sections of the pseudo-shock increases as the boundary layer thickness at the initial section increases,

$$\frac{P_2}{P_1} = \frac{\zeta_1 w_1}{1 - \eta_1 {w_1}^2} \frac{1 - \eta_2 {w_2}^2}{\zeta_2 w_2} \tag{13}$$

where ζ and η are the correction factors for the mass flux and energy respectively in the integral equations of continuity and conservation of energy.

Matsuo et al.[90] proposed a *mass averaging pseudo-shock model* for a constant area duct with a fully turbulent boundary layer. This model, expressed by Equation 14, is able to explicitly obtain the flow properties across the pseudo-shock and predicts the static pressure rise and total pressure loss with good accuracy, particularly for high Mach numbers,

$$\frac{P_2}{P_1} = \frac{\bar{M}_1}{\sigma_1 M_2} \left[\frac{2 + (\gamma - 1)\, \bar{M}_1^2}{2 + (\gamma - 1)\, \bar{M}_2^2} \right]^{1/2} \tag{14}$$

with:

$$\sigma = \frac{\bar{\rho}\bar{u}A}{\int \rho u \; dA} \tag{15}$$

The only analytical expression which relates the pressure gradient experienced by the flow along a duct in the presence of separated regions and the length required to achieve the full pressure rise was proposed by Ortwerth.[91] Referring to Figure 29, the core flow in region I, subject to a pressure gradient due to the area restriction caused by the separated flow (region III), passes through the shock train and expands through an area increase after being decelerated to subsonic conditions. The formula, given by Equation 16, was determined from a comprehensive experimental campaign at different Mach numbers, Reynolds numbers and duct geometries, and hence is applicable to a wide range of flow conditions and geometries,

$$\frac{d\,(P/P_1)}{dx} = 4K \; \gamma \; P/P_1 \; M^2 \tag{16}$$

where $4K = 44.5 \; C_{f0}$, in which C_{f0} is the friction coefficient at the location where the flow initially separates. This equation can be used to close the system of differential equations of mass, momentum, and energy in the presence of flow separation to predict the pressure distribution in the entire region of the duct. Equation 16 was used by Tu & Segal[92] with two values for the wall friction coefficient, $C_{f0} = 0.01$ and 0.005, finding a strong dependence of the model accuracy on the selection of the friction coefficient. As Figure 30 illustrates, the value of 0.005 underpredicts the pressure rise, and even though the 0.01 value initially matches the experimental data, it later gradually diverges.

A *non-optimal ramjet-diffuser model* proposed by Auslender[93] consistent with the experimental data obtained by Emami et al.[50] improved the estimation of the static pressure distribution throughout the diffuser and the maximum-obtainable values.

Lin et al.[74] obtained a linear relationship between the centreline Mach number M_{CL} at the isolator exit with the pressure ratio downstream and upstream of the isolator P_2/P_1. Although two different correlations were developed for rectangular and circular isolators in Equation 17 and Equations 18 respectively, the centreline Mach number linearly decreases with back pressure. Additionally, for a given value of the back pressure, the circular geometry provides higher centreline Mach numbers, as Figure 31 illustrates.

$$\frac{M_{CL}}{M_0} = -1.17\ {M_0}^{-2.40} \left(\frac{P_2}{P_1}\right) + 1.78\ {M_0}^{-0.64} \tag{17}$$

$$\frac{M_{CL}}{M_0} = -0.94\ {M_0}^{-2.20} \left(\frac{P_2}{P_1}\right) + 1.60\ {M_0}^{-0.48} \tag{18}$$

The majority of investigations of shock trains have been performed neglecting the wall temperature effects. A recent study carried out by Fischer & Olivier[94] showed that in cases with low total temperature or high isolator entrance Mach number, the shock train is made of several weak shocks and the pressure rise exhibits a linear trend. On the other hand, for high total temperature or low isolator entrance Mach numbers conditions, a well-defined first shock is observed in front of the shock trains. In this case, due to the steeper pressure gradient at the beginning of the shock train, the pressure rises with a quadratic correlation. This shows the inadequacy of the models that do not account for wall temperature effects in those cases when the isolator wall is heated. However, as stated by the authors, the validity of the suggested modification where demonstrated only for a limited range of flow condition and geometry.

The current understanding on the mechanisms of the pseudo-shock phenomenon is not sufficient and an accurate estimation of the pressure distribution across the isolator needs to be formulated to obtain a reliable prediction of the pseudo-shock in internal flow systems. More accurate two- or three-dimensional flow description, including transverse pressure gradients, heat transfer, and flow unsteadiness, can be achieved with numerical simulation. From the 1980s, the growth in computer speed and storage capabilities combined with the development of sophisticated algorithms has allowed the use of numerical codes as a valuable tool for analysing the structure of internal flows.[95]

Numerical codes have shown to be promising and satisfactory results have been obtained. Mousavi and Roohi[96] were able to well predict the shape of the first shock wave, as illustrated in Figure 32. However, differences with experimental data are still encountered.[24] As an example illustrated in Figure 33, the pressure distribution inside a scramjet isolator obtained by Baurle et al.[97] showed some discrepancies between measured and real flow. The experimental pressure distribution monotonically increases through the shock train while the computed data show an oscillatory behaviour. In addition, all the numerical models employed failed to accurately predict the shape and the extent of the separated flow region

caused by the shock/boundary layer interactions.

The choice of the proper numerical code is sometimes guided by conflicting issues, such as the need for an accurate and detailed design which opposes low costs and low simulation time requirements.[98] The computational modelling of compressible flows is in general quite difficult because of the challenging behaviour of the shock-train and shock/boundary layer interactions, and various numerical techniques have been developed to analyse air-breathing propulsion.[99] A great amount of numerical work has been performed in this area,[100–104] but a detailed review of the numerical achievements and status is beyond the scope of this effort.

V. SHOCK WAVE/BOUNDARY LAYER INTERACTION CONTROL

Shock wave/boundary layer interactions are frequently present on a variety of flow fields such as aerofoils, aircraft engines, and high-speed vehicles.[105–107] As already explained, in a hypersonic inlet, the velocity reduction from the freestream value is obtained through an efficient sequence of shock waves which impinge on the walls of the inlet frame, interacting with the boundary layer. Excessive blockage or an asymmetric entrance condition can aggravate the diffuser flow and boundary layer separation which often cause a drastic decrease of the inlet performance and flow stability.[108] The unstart process is at a high level associated with a pressure rise due to combustor heat release that is too high for the approach boundary layer flow to withstand. As observed by Im et al.,[109] the boundary-layer characteristics and separation strongly affect the unstart process. To counteract the negative effects of shock wave/boundary layer interactions, adequate manipulation of the boundary layer development and separation is necessary.[30,110] Although several flow control techniques have been successfully applied to low-speed flows, the use in the high-speed regime remains limited and a topic of future research.[111] Flow control techniques make use of different physical principles and are generally classified as passive control and active control. In passive control techniques, one or more sections of the surface structure is used to modify the flow and thus control boundary layer separation. On the contrary, active control techniques employ a powered device which adds energy to the flow and can be switch on and off depending on the need.[108]

One possibility to control the behaviour of the boundary layer is the use of passive bleeding. This method was firstly applied by Prandtl[112] in 1904 to prevent separation in a channel

with a large angle of divergence, and since then many bleeding configurations for supersonic inlets have been developed and optimised.[113] In general, bleeding has been demonstrated to be effective in reducing boundary layer separation at the shock impingement location, improving shock stability, and increasing the pressure recovery and the pressure limit to separation.[114,115] By using a bleeding device, Weise[116] was able to remove the boundary layer separation observing the flow pattern changing from the shock train into a single normal shock configuration, as Figure 36 illustrates.

In a bleeding system, such as the example of a double-cone supersonic inlet in Figure 37, a bleed slot is located between the start and end points of a shock wave, with a bleed plenum installed under the bleed slot. Compared to a supersonic inlet without bleeding, a more uniform flow is supplied to the engine by removing the low energy flow from the boundary layer near the throat. As illustrated in Figure 38, by changing the cross-sectional area of the sonic throat, the critical mass flow rate of the bleeding system can be controlled.

The drawback of bleeding is that a significant fraction of the ingested inlet mass flow is removed[117] and, as reported by Harloff & Smith,[118] the flow removal increases with the Mach number. For high-speed systems, another big problem that affects structural integrity is the temperature of the flow being bled due to extreme viscous heating in hypersonic boundary layers.[119,120] Paynter et al.[121] found that boundary layer growth rate in the bleed region is influenced by the combined effect of the surface roughness and the mixing of high- and low-energy air in the boundary layer so that they developed an algebraic model to relate the surface roughness with the fraction of the boundary layer mass flux removed with bleed. However, the mechanism responsible for bleed roughness is difficult to quantify. Several analytical, experimental, and computational studies have been performed to determine methodologies to optimise the bleed-hole pattern or slot geometry since the efficiency of this method depends on the local Mach number, pressure ratio, and hole shape or slot length-to-diameter ratio.[122–124] Additionally, the entire bleeding system significantly increases the auxiliary complications in the inlet design due to movable compression ramps and slots controlled by sophisticated software or mechanical systems. These complications increase with the speed of the aircraft and, as Saha & Chakraborty[103] stated, in flow situations with high total temperature ($\sim$ 1800 K), any complex mechanical control system may cause severe structural and cooling problems.

Similarly to bleeding, porous walls located at the position were the shock impinges the

wall is used as a flow control method.[108] The main advantage of this approach is the reduction of design sophistication and volume penalties since no mass removal and bleed ducting are required.[125] At the interaction region, the flow is injected upstream of the shock and sucked downstream, establishing a natural circulation within the enclosed cavity.[126] The pressure difference across the shock is thus spread more uniformly and the flow is compressed in a more isentropic way, with a consequent greater pressure recovery behind the shock wave.[127]

The use of streamwise slots placed at the position where a normal shock wave interacts with the boundary layer appears to be effective for a range of shock locations compared to the aforementioned methods which exhibit decreasing benefits in off-design conditions.[128] Since the effect of slots on the boundary layer is localised to the region behind the slots, lower viscous penalties and total pressure loss are observed compared to conventional wall transpiration. On the other hand, the boundary layer displacement and momentum thickness are subject to detrimental effects, which then increase the viscous drag.[129]

Gefroh et al.[126] combined this concept with aeroelastic flaps to balance the two opposing tendencies of recirculating transpiration. The system, called mesoflaps for aeroelastic recirculating transpiration (MART), consists of small flaps with a scale length of the order of few boundary layer thicknesses to passively control injection and bleeding. As illustrated in Figure 39, the flaps are rigidly fixed at their upstream end but free to deform at the downstream end in response to a pressure difference which establishes between the supersonic flow and the cavity subsonic flow. Since at subsonic conditions the pressure above and below the mesoflaps is nearly the same no deflection occurs, therefore no transpiration is induced from the slots to the surface which means that surface roughness present in conventional passive control techniques at off-design conditions is minimised at this location. This device reduces the boundary layer thickness downstream of the shock and improves its efficiency with increasing flap deflection due to the larger flow recirculation rate. Hafenrichter et al.[130] studied different configuration of the flap arrays as well as various mesoflap thickness finding that the thickness, and consequently the deflection and the transpiration rate, affect the boundary layer integral properties, and the static and total pressure recovery. Despite the fact that some of the arrays did not have beneficial effects, the thickness of the mesoflap demonstrated to have a greater impact on performance when the array was changed from a four-flap to a six-flap configuration.

Srinivasan et al.[129] experimentally compared the effect of conventional porous plate, mi-

croporous plate, streamwise slots, a conventional mesoflap array, and a hybrid flap array. The hybrid flaps were designed with the purpose to combine the benefits of MART with streamwise slots for promoting streamwise vorticity but the desired benefits were not obtained and the authors concluded that the strength of the streamwise vortices generated from the flap edges were lower compared to the slots. The flow was found to be mainly two-dimensional downstream of the macroporous, microporous, and mesoflap array, whereas streamwise slots and hybrid flap arrays are characterised by three-dimensional structures. Additionally, all the control devices tested generated lambda shocks of larger size with stronger destabilisation effects on the boundary layer compared to the baseline solid wall.

Another mechanism to manipulate boundary layer separation due to adverse pressure gradients is the use of boundary layer trips to promote turbulence.[9] Vortex generators (VGs) have been used in a wide range of aviation applications spanning from the wings of civil aircrafts to the intakes of supersonic jet engines, to reduce fluctuating pressure loads for buffet control[131] or delay flow separation.[132] Micro Vortex Generators (MVGs), also referred to sub-boundary layer vortex generators (SBVGs), characterised by having a height smaller than the boundary layer thickness ($10\% - 90\%\ \delta$[108]), have been proposed to mitigate the adverse effects of shock wave/boundary layer interaction.[133,134] MVGs are particularly effective in controlling flow separation, in producing a slightly thicker boundary layer and having a lower drag penalty than conventional generators, even though they cannot eliminate separation completely.

VGs act by energising the boundary layer, i.e. enhancing the mixing process between the high-momentum external flow and the low-momentum near-wall flow and alleviate the shock interaction.[127] These devices, initially introduced in the 1940s, work by developing counter-rotating longitudinal vortices in the near-wall region.[135] These vortices remain in the boundary layer for a significant streamwise distance, so that higher pressure gradients can be tolerated before separation and, if separation occurs, the vortices generated accelerate reattachment.[114] On the other hand, this method presents the disadvantage to increase parasitic drag, which increases with the device size. The flow development behind VGs scales with their height, i.e. larger microramps lead to a greater low-momentum wake, and larger and stronger vortices.[133] Holden & Babinsky[131] studied the spatial arrangement of VGs and found that, depending on the configuration, different levels of control of the shock-induced separation and total pressure loss are achievable. As shown in Figure 40, an array of

microramps along the spanwise direction demonstrated higher performance compared to the single configuration, although an optimum spanwise spacing has not yet been established.[133]

A promising passive method of shock control is the so-called shock control bumps (SCBs),[136] firstly investigated by Ashill et al.[137] It consists of placing a ramp in proximity of the location where the shock wave impinges on the wall but, due to the presence of the boundary layer, a λ shock structure takes place, as Figure 41(a) illustrates. As shown in Figures 41(b) and 41(c), this device has the effect to split the normal shock wave into a number of weaker oblique or compression waves ahead of the shock, followed by a tail which is necessary to bring the flow downstream of the shock parallel to the surface.[138] The premise of this strategy relies on the fact that the total pressure loss across multiple oblique shock waves is smaller than that across a normal shock with the same pressure jump, with the consequent achievement of an overall mitigated effect.

Although the use of SCBs has demonstrated a significant reduction in drag at design conditions, considerable penalties in performance have been reported when the shock position varies, namely in off-design cases. Figure 42(b) shows the optimal configuration characterised by a large λ shock without additional total pressure losses which occur when the shock structure is positioned too far upstream, causing secondary shock systems, or too far downstream, causing boundary layer thickening, as illustrated in Figures 42(a) and 42(c) respectively.

Lim et al.[139] replaced the compression ramp used in conventional supersonic inlets with a three-dimensional bump, which not only enhanced the control of shock wave/boundary layer interaction, but also showed the important role of the bump geometrical characteristics. Similar conclusions were reported by Ogawa & Babinsky,[140] who investigated several bump configurations, as shown in Figure 43. Zhang et al.[141] recently studied a deformable two-dimensional bump which appears only when the supersonic/hypersonic inlet operates at a high Mach number, but disappears at low Mach number so that the duct height is increased for the inlet starting. However, as pointed out by the authors, the effects of this device deteriorate at off-design conditions, and therefore the use of such a control method during flight is questionable.

The sensitiveness of fluids to musical tones has been detected since the middle of the 19th century when it was observed that regular aerial pulsations generated by musical notes are sufficient to develop synchronised fluctuations in a candle flame.[142] Later on it was

discovered that this is due to the fact that noise propagates in the air by pressure waves and, more recently, it has been recognised that the combustor performance in aircraft engines is influenced by the fuel injection mode. The introduction of air or fuel along the walls has therefore been used to reduce the low-momentum flow in the boundary layer, thus alleviating separation and heat transfer problems inside the isolator. Qin et al.[143] numerically investigated the effect of fuel injection on the pseudo-shock finding that the variations of shock structure, strength and leading edge position depend on the way the fuel is injected. Also, if the level of asymmetric fuel injection is too high, the isolator unstarts. Steady microjets have experimentally been shown to be effective on flow control, particularly in reattaching large separated regions.[144,145] Resonance enhanced microjets (REM) produce large amplitude oscillations and operate over a wide bandwidth, even with slight geometry and pressure changes.[146,147]

It is worth mentioning that the pseudo-shock wave characteristics and control have been used to enhance the fuel/air mixing and increase the combustion efficiency when the fuel is perpendicularly injected in the main stream.[2,55,148–150] When subjected to back pressure, the isolator flow is characterised by an increase in temperature and decrease in gas velocity providing a highly non-uniform favourable environment for the fuel/air mixing and flame ignition inside the combustor.[74]

Surface electrical discharges, with a plasma filament placed between the anode and the cathode located upstream of the shock interaction with the boundary layer, called localised arc filament plasma actuators (LAFPAs), can also be employed for manipulating the flow.[151] The arc discharge which occurs between the two electrodes gives rise to the formation of plasma in the arc channel within the gas. Across this gap the electrons are accelerated by the electric field, gaining the energy to collide with the gas molecules thus enhancing the ionization and producing more electrons. According to Samimy et al.,[152] localised arc-generated pressure/temperature flow perturbations can be efficiently employed not only to low-speed or low-pressure flows but also in high Reynolds number and high-speed flows with low energy consumption, large amplitude and high bandwidth. Caraballo[135] observed that the unsteady nature of the leading leg of the λ shock wave, which forms as a consequence of the shock wave/boundary layer interaction, can be controlled by forcing the flow with LAFPAs, as Figure 44 illustrates.

Mechanisms of plasma flow control include electrohydrodynamic (EHD) and magneto-

hydrodynamic (MHD) interactions, and thermal heating.[153,154] The first two methods rely on the Lorentz force generated by an adjustable magnet located at the inlet in the presence of plasma to change the flow direction and control the boundary layer.[152] The heated region creates local thermal and pressure perturbations which act as a bump in the flow, thus generating streamwise vortices which transfer the high-energy freestream flow into the boundary layer.

Roupassov et al.[155] reported that, to control boundary layer separation at low Mach number flows, a nanosecond pulsed voltage is more efficient compared to sinusoidal excitations. This is in agreement with Ali et al.,[146] who observed that high-amplitude pulsed actuators are more efficient than the same kind of actuator operating in steady mode, and Adelgren et al.,[156] who demonstrated that the frequency control of the electrical arc perturbation enhances the mixing of a supersonic jet within the shear layer and induces the formation of large-scale structures.

Pulse plasma jets, also called spark jets, are a mix between arc filament plasma actuators and air jets. The jet pulse is driven by an electrical discharge in a plenum chamber that rapidly heats the gas, which in turn expands out of the exit and generates a rarefaction wave which refills the chamber for the next pulse.[157] The effectiveness of pulsed plasma jets in reducing the separation bubble in proximity of the foot of the shock wave was found dependent on the electrical design parameters as well as the jets configuration in terms of pitch angle, number of jets, and distance between two consecutive jets.[108,111] Narayanaswamy et al.[158] concluded that plasma jet actuators may be an effective option to control the shock wave/boundary layer interaction by shifting the dominant oscillation frequency of separated flows to avoid the coupling with the structural resonance frequencies.

Plasma flow control technology is currently one of the most advanced approaches to control a wide range of flows, from stationary to separated and turbulent, with a fast reaction time, and low weight and size.[155] The majority of experiments have demonstrated a high efficiency in controlling shock wave patterns, separated regions, and laminar/turbulent transitions.[159–161] However, the prohibitively high energy storage unit required by a plasma-exciting device and the limitation due to ionization instabilities, in addition to the problems related to the interference of the radio communication and flight guidance generated, do not allow the application of plasma control to real flow devices.[152,162]

The location of the shock train leading-edge in the isolator can be used as an input

variable in an automatic feedback controller. Initial methodologies to detect the shock train leading edge relied on the increase of the wall pressure. The approach was then developed further introducing statistical parameters including the pressure ratio, pressure root mean square intensity, pressure signal spectral analysis, static pressure summation model, and back pressure static model.[36,163] Among several methods, Le et al.[164] found the standard deviation of wall pressure to be the best way of determining the shock train leading-edge location in the isolator for operational applications. Chang et al.[165] developed a detection algorithm based on the pressure signal profile given by a large number of sensor probes, which is compared with a reference value, to design the optimal pressure sensor array capable to detect the shock train leading-edge location. Although this principle appears simple, the reference value needs to be constantly modified depending on flight conditions, inlet geometry, angle of attack, and yaw. Additionally, the accuracy of the measured data may be perturbed by the noise introduced by shocks reflections as well as the limitation due to the discrete sensor distribution, which requires polynomial interpolation to obtain the signal where no sensors are available.

The various methods developed to control the interaction of the boundary layer with a shock wave have attempted to achieve suppression of boundary layer separation or reduction of total pressure losses with simple and robust actuator systems, easily integrated with the geometry. All the discussed techniques offer advantages and disadvantages and, even though some are more suitable for high-speed inlet applications than others, none are able to fulfil the goal without incurring significant installation or operating penalties.[146] Since vortex generators improve the boundary layer downstream of the shock and suppress the separation region, these devices are particularly suitable for supersonic intake applications, in spite of the fact that a lower mass-averaged total pressure is obtained downstream of the shock.[127]

VI. CONCLUSIONS

The use of air-breathing engine cycles to power high-speed aircraft has acquired growing importance and attracted the attention of the research community for many years. Ramjets and scramjets appear to be an important configuration for future aerospace vehicles and to fulfil the need to substantially improve efficiency, reduce trip times and emissions compared to subsonic aircrafts, and promote reusability in rocket design. One of the main goals for

air-breathing propulsion is the possibility to design a completely reusable, single-stage space plane, able to take off and land without the aid of another vehicle.

Currently air-breathing vehicles are characterised by a high level of integration between the propulsion system and the vehicle frame. Before the air flow arrives at the combustion chamber, it must be slowed down to lower supersonic speeds (in scramjets) or to subsonic speeds (in ramjets) by means of shock waves and mixed compression located inside the isolator. As the Mach number increases, the shock structure evolves from a single normal shock towards multiple oblique shocks, and boundary layer separation becomes more likely due to shock wave/boundary layer interactions.

In spite of the technological advances in the last fifty years, the shock train and the pseudo-shock phenomena are extremely complex and still not well understood. Simplifications in describing the flow structure have been introduced to reduce the difficulties encountered in the flow description. The reduced complexity not only has been identified as the source of inconsistency between experimental and analytical results but also limited the complete description of the flow phenomena.

The majority of the analytical formulations have primarily focused on the prediction of the maximum static pressure recovery. Empirical expressions have been introduced to relate the distance over which the shock structure is spread with the flow parameters. However the dependence of these expressions on the flow characteristics such as the boundary layer momentum thickness requires a great amount of experimental data for an accurate estimation. Additionally, some analytical expressions can be applied only to cylindrical ducts, and experimenetal data have been mostly limited to constant area ducts and symmetric conditions. Therefore, the validatation of models applicable to rectangular geometry has been particularly challenged and the current knowledge about rectangular cross-sections still presents gaps. The only analytical expression which relates the pressure gradient experienced by the flow along a duct in the presence of separated regions and the length required to achieve the full pressure rise was proposed by Ortwerth.[91] The accuracy of this model has demonstrated to be strongly dependent on the values for the wall friction coefficient. The inadequacy of the analytical models becomes significant if the isolator wall is heated because the shock train changes its behaviour. In consequence of this, more accurate models applicable to a wider range of flow and geometry conditions are necessary.

Simulations have become an important tool in the design stage of high-speed vehicles

since above Mach 12 the reproduction of the flow conditions at ground test facilities is challenging. Even though the agreement between computations and experimental data are increasingly improving, numerical flow fields are limited by the choice of the flow models and the numerical algorithms employed. Additionally, since most numerical calculations are based on time-mean flow physics the shock train oscillating behaviour is not satisfactorily reproduced. More accurate flow models must be employed, including an accurate application of transverse pressure gradients, heat transfer and flow unsteadiness. As a result, experimental results remain an invaluable resource not only for validating numerical simulation, but also for the understanding of the physical flow behaviour.

Several flow control techniques have been proposed to manipulate the shock wave/boundary layer behaviour but none have been found suitable for high-speed inlets without drawbacks and therefore further investigations are needed.

ACKNOWLEDGMENTS

This work was supported by the Engineering and Physical Sciences Research Council and the staff at the University of Glasgow.

[1] McLafferty, G., "Theoretical Pressure Recovery Through a Normal Shock in a Duct with Initial Boundary Layer," *Journal of the Aeronautical Sciences* **20(3)**, 169–174, (1953).

[2] Yamauchi, H., Choi, B., Kouchi, T., Masuya, G., "Mechanism of Mixing Enhanced by Pseudo-Shock Wave," *AIAA paper 2009-25*, (2009).

[3] Gibbs-Smith, C.H., "Aviation: an historical survey from its origins to the end of World War II," *H.M.S.O.*, London (2009).

[4] Fry, R.S., "A Century of Ramjet Propulsion Technology Evolution," *Journal of Propulsion and Power* **20(1)**, 27–58, (2004).

[5] Taylor, M.J.H., Taylor, J.W.R., Gunston, B., "Jane's encyclopedia of aviation," *Jane's, London*, (1980).

[6] Gunston, B., "Chronicle of aviation," *Chronicle Communications*, London (1960).

[7] Gibbs-Smith, C.H., "The aeroplane: a historical survey of its origins and development," *H.M.S.O.*, London (1960).

[8] Ferri, A., Nucci, L.M., "Preliminary investigation of a new type of supersonic inlet," *NACA-TN-2286*, (1951).

[9] Swithenbank, J., "'Hypersonic air-breathing propulsion," *Progress in Aerospace Sciences* **8**, 229–294, (1967).

[10] Sullins, G.A., "Demonstration of mode transition in a scramjet combustor," *Journal of Propulsion and Power* **9(4)**, 515–520, (1993).

[11] Curran, E.T., Heiser, W.H., Pratt, D.T., "Fluid phenomena in scramjet combustion systems," *Annual Review of Fluid Mechanics* **28**, 323–360, (1996).

[12] Timnat, Y.M., "Recent developments in ramjets, ducted rockets and scramjets," *Progress in Aerospace Sciences* **27(3)**, 201–235, (1990).

[13] Sullins, G., "Experimental Results of Shock Trains in Rectangular Ducts," *AIAA-92-5103*, (1992).

[14] Bement, D.A., Stevens, J.R., Thompson, M.W., "Measured operating characteristics of a rectangular combustor/inlet isolator," *AIAA/SAE/ASME/ASEE 26th Joint Propulsion Conference* **90-2221**, (1990).

[15] Billig, F.S., Corda, S., Pandolfini, P.P., "Design Techniques for Dual Mode Ram Scramjet Combustors" *AGARD 75th symposium of hypersonic combined cycle propulsion, Madrid, 1990* **23**, 23-1–23-20, (1990).

[16] Smart, M.K., "Scramjets," *Advances on Propulsion Technology for High-Speed Aircraft*, 9-1–9-38,

(2008).

[17] Smart, M.K., "How much compression should a scramjet inlet do?," *AIAA Paper* **50(3)**, 610–619, (2012).

[18] Wagner, J.L., Yuceil, K.B., Clemens, N.T., "Velocimetry measurements of unstart in an inlet isolator model in Mach 5 flow," *AIAA Journal* **48(9)**, 1875–1888, (2009).

[19] Wagner, J.L., Yuceil, K.B., Clemens, N.T., Dolling, D.S., "Experimental investigation of unstart in an inlet/isolator model in Mach 5 flow," *AIAA Journal* **47(6)**, 1528–1542, (2009).

[20] Tao, C., Daren, Y., Juntao, C., Wen, B., "Topological geometry interpretation of supersonic inlet start/unstart based on catastrophe theory," *Journal of Aircraft* **45(4)**, 1464–1468, (2008).

[21] Huang, W., Wanga, Z., Pourkashanian, M., Mab, L., Ingham, D.B., Luo, S., Lei, J., Liu, L., "Numerical investigation on the shock wave transition in a three-dimensional scramjet isolator," *Acta Astronautica* **68(11-12)**, 1669–1675, (2011).

[22] Billig, F.S., "Combustion processes in supersonic flow," *Journal of Propulsion and Power*, **4(3)**, 209–216, (1988).

[23] Crocco, L., "High Speed Aerodynamics and Jet Propulsion," *Princeton University Press* **3**, Princeton, (1958).

[24] Matsuo, K., Miyazato, Y., Kim, H.D., "Shock train and pseudo-shock phenomena in internal gas flows," *Progress in Aerospace Sciences* **35**, 33–100, (1999).

[25] Squire, L.C., "Interaction of swept and unswept normal shock waves with boundary layers," *AIAA journal* **34(10)**, 2099–2101, (1996).

[26] Om, D., Childs, M.E., "Multiple Transonic Shock-Wave/Turbulent Boundary-Layer Interactions in a Circular Duct," *AIAA journal* **23(10)**, 1506–1511, (1985).

[27] Gawehn, T., Gülhan, A., Al-Hasan, N.S., Schnerr, G.H., "Study on Shock Wave and Turbulent Boundary Layer Interactions in a Square Duct at Mach 2 and 4," *Shock Waves* **20**, 297–306, (2010).

[28] Om, D., Childs, M.E., Viegas, J.R., "Transonic Shock-Wave/Turbulent Boundary-Layer Interactions in a Circular Duct," *AIAA journal* **23(5)**, 707–714, (1985).

[29] Lustwerk, F., "The Influence of Boundary Layer on the 'Normal' Shock Configuration," *Massachusetts Institute of Technology, Guided Missiles Program*, (1950).

[30] Babinsky, H., Harvey, J.K., "Shock Wave-Boundary-Layer Interactions," *Cambridge University Press*, Cambridge, (2011).

[31] Weiss, A., Grzona, A., Olivier, H., "Behavior of shock trains in a diverging duct," *Experiments in Fluids*

49(2), 355–365, (2010).

[32] Merkli, K., "Pressure Recovery in Rectangular Constant Area Supersonic Diffusers," *AIAA Journal* **14(2)**, 168–172, (1976).

[33] Neumann, E.P., Lustwerk, F., "High-Efficiency Supersonic Diffusers," *Massachusetts Institute of Technology, Guided Missiles Program, Issue 56 of Meteor report*, (1950).

[34] Fischer, C., Olivier, H., "Experimental Investigation of the Internal Flow Field of a Scramjet Engine," *AIAA Paper 2009-7369*, 1657–1667, (2009).

[35] Ikui, T., Magai, M., Matsuo, K., "The Mechanism Of Pseudo-Shock Waves," *Bulletin of the JSME* **17(108)**, 731–739, (1974).

[36] Sajben, M., Donovan, J.F., Morris, M.J., "Experimental investigation of terminal shock sensors for mixed-compression inlets," *Journal of Propulsion and Power* **8(1)**, 168–174, (1992).

[37] Lukasiewicz, J., "Diffusers for Supersonic Wind Tunnels," *Journal of the Aeronautical Sciences* **20(9)**, 617–626, (1953).

[38] Sugiyama, H., Minato, R., Mizobata, K., Tojo, A., Muto, Y., "Experimental and numerical analysis of the structure of pseudo-shock systems in Laval nozzles with parallel side walls," *Journal of Thermal Science* **15(1)**, 37–42, (2006).

[39] Hataue, I., "Computational study of the shock-wavey/boundary-layer interaction in a duct," *Fluid Dynamics Research* **5(3)**, 217–234, (1989).

[40] Sun, L. Sugiyama, H., Mizobata, K., Minato, R., Tojo, A., "Numerical and experimental investigations on Mach 2 and 4 pseudo-shock waves in a square duct," *Transactions of the Japan Society for Aeronautical and Space Sciences* **47(156)**, 124–130, (2004).

[41] Heiser, W.H., Pratt, D.T., "Hypersonic airbreathing propulsion," *American Institute of Aeronautics and Astronautics*, Washington, D.C., (1994).

[42] Carroll, B.F., Lopez-Fernandez, P.A., Dutton, J.C., "Computations and experiments for a multiple normal shock/boundary-layer interaction," *Journal of Propulsion and Power* **9(3)**, 405–411, (1993).

[43] Ostras, V.N., Penzin, V.I., "Experimental Study of Friction in a Channel with Pseudoshock," *Fluid Mechanics* **4(6)**, 32–38, (1975).

[44] Nagai, M., "Mechanism Of Pseudo-Shock Wave in Supersonic Jet," *Bulletin of the JSME* **26(212)**, 207–214, (1983).

[45] Sun, L.Q., Sugiyama, H., Mizobata, K., Fukuda, K., "Experimental Investigations on the Mach 2 Pseudo-Shock Wave in a Square Duct," *Shock Waves* **6(4)**, 363–370, (2003).

[46] Ikui, T., Magai, M., Matsuo, K., Sasaguchi, K., "Modified Diffusion Model of Pseudo-Shock Waves Considering Upstream Boundary Layers," *Bulletin of the JSME* **24(197)**, 1920–1927, (1981).

[47] Reinartz, B.U., Herrmann, C.D., Ballmann, J., "Performance Analysis of a Hypersonic Inlet Isolator Using Computation and Experiment," *Journal of Propulsion and Power* **19(5)**, 868–875, (2003).

[48] Mahoney, J.J., "Inlets for supersonic missiles," *American Institute of Aeronautics and Astronautics*, Washington, D.C., 55–66, (1990).

[49] McLafferty, G.H., Krasnoff, E.L., Ranard, E.D., Rose, W.G., Vergara, R.D., "Investigation of Turbojet Inlet Design Parameters," *United Aircraft Corporation, Research Laboratories*, (1955).

[50] Emami, S., Trexler, C.A., Auslender, A.H., Weidner, J.P., "Experimental Investigation of Inlet-Combustor Isolators for a Dual-Mode Scramjet at a Mach Number of 4," *NASA Technical Paper 3502*, (1995).

[51] Ikui, T., Matsuo, K., Nagai, M., Honjo, M., "Oscillation Phenomena of Pseudo-Shock Waves," *Bulletin of the JSME* **17(112)**, 1278–1285, (1974).

[52] Matsuo, K., Mochizuki, H., Miyazato, Y., Gohya, M., "Oscillatory characteristics of a pseudo-shock wave in a rectangular straight duct," *JSME International Journal Series B* **36(2)**, 222–229, (1993).

[53] Kim, H.D., Matsuo, K., Kawagoe, S., Kinoshita, T., "Flow unsteadiness by weak normal shock wave/turbulent boundary layer interaction in internal flow," *JSME International Journal Series II* **34(4)**, 457–465, (1991).

[54] Handa, T. Mitsuharu, M.,Matsuo, K., "Three-Dimensional Normal Shock-Wave/Boundary-Layer Interaction in a Rectangular Duct," *AIAA Journal* **43(10)**, 2182–2187, (2005).

[55] Yamauchi, H., Choi, B., Takae, K., Kouchi, T., Masuya, G., "Flowfield characteristics of a transverse jet into supersonic flow with pseudo-shock wave," *Shock Waves* **22(6)**, 533–545, (2012).

[56] Yamane, R., Kondo, E., Tomita, Y., Sakae, N., "Vibration of pseudo-shock in straight duct, 1st Report, Fluctuation of static pressure," *Bulletin of the JSME* **27(229)**, 1385–1392, (1984).

[57] Yamane, R., Takahashi, M., Saito, H., "Vibration of pseudo-shock in straight duct, 2nd Report, Correlation of static pressure fluctuation," *Bulletin of the JSME* **27(229)**, 1393–1398, (1984).

[58] Sugiyama, H., "Locations And Oscillation Phenomena Of Pseudo-Shock Waves In A Straight Rectangular Duct," *JSME International Journal, Series B: Fluids and Thermal Engineering* **31(1)**, 9–15, (1988).

[59] Robinet, J.C., Casalis, G., "Shock Oscillations in Diffuser Modeled by a Selective Noise Amplification," *AIAA Journal* **37(4)**, 453–459, (1999).

[60] Su, W.Y., Zhang, K.Y., "Back-Pressure Effects on the Hypersonic Inlet-Isolator Pseudoshock Motions," *Journal of Propulsion and Power* **29(6)**, 1391–1399, (2013).

[61] Hsieh, T., Coakley, T.J., "Downstream Boundary Effects on the Frequency of Self-Excited Oscillations in Diffuser Flows," *AIAA Paper 87-0161*, (1987).

[62] Bogar, T.J., Sajben, M., Kroutil, J.C., "Characteristics frequencies of transonic diffuser flow oscillations," *AIAA Journal* **21(9)**, 1232–1240, (1983).

[63] Bogar, T.J., "Structure of self-excited oscillations in transonic diffuser flows," *AIAA Journal* **24(1)**, 54–61, (1986).

[64] Xiao, Q., Tsai, H.M., Papamoschou, D., "Numerical Investigation of Supersonic Nozzle Flow Separation," *AIAA Journal* **45(3)**, 532–541, (2007).

[65] Papamoschou, D., Zill, A., "Fundamental Investigation of Supersonic Nozzle Flow Separation," *AIAA Paper 2004-1111*, (2004).

[66] Papamoschou, D., Johnson, A., "Unsteady Phenomena in Supersonic Nozzle Flow Separation," *AIAA Paper 2006-3360*, (2006).

[67] Kawatsu, K., Koike, S., Kumasaka, T., Masuya, G., Takita, K., "Pseudo-Shock Wave Produced by Backpressure in Straight and Diverging Rectangular Ducts," *AIAAPaper 20053285*, (2005).

[68] Hsieh, T., Wardlaw, A. B., Coakley, T., "Ramjet diffuser flowfield response to large-amplitude combustor pressure oscillations," *Journal of Propulsion and Power* **3(5)**, 472–477, (1987).

[69] Oh, J.Y., Ma, F., Hsieh, S.Y., Yang, V., "Interactions Between Shock and Acoustic Waves in a Supersonic Inlet Diffuser," *Journal of Propulsion and Power* **21(3)**, 486–495, (2005).

[70] Cohen, C.B., Valerino, A.S., "Investigation of operating pressure ratio of a supersonic wind tunnel utilizing distributed boundary-layer suction in test section," *NACA Research Memorandum E50H04*, (1950).

[71] Ikui, T., Matsuo, K., Mochizuki, H., Somekawa, K., "Pseudo-shock waves in a divergent channel," *Bulletin of the JSME* **23(175)**, 20–25, (1980)..

[72] Neumann, E.P., Lustwerk, F., "Supersonic Diffusers for Wind Tunnels," *Journal of Applied Mechanics* **16(2)** , 195–202, (1949).

[73] Walther, R., Koschel, W., Sabelnikov, V., Korontsvit, Y., Ivanov, V., "Investigations into the Aerothermodynamic Characteristics of Scramjet Components," *International Society for Air Breathing Engines* **97-7085**, 463–473, (2008).

[74] Lin, K.C., Tam, C.J., Jackson, K.R., Eklund, D.R., Jackson, T.A., "Characterization of Shock Train

Structures Inside Constant-Area Isolators of Model Scramjet Combustors," *AIAA Paper 2006-0816*, 1442–1452, (2006).

[75] Sridhar, T., Chandrabose, G., Thanigaiarasu, S., "Numerical Investigation of Geometrical Influence On Isolator Performance," *IJTARME* **2**, 7–12, (2013).

[76] Green, J.E., "Interactions between shock waves and turbulent boundary layers," *Progress in Aerospace Sciences* **101**, 235–340, (1970).

[77] Cuffel, R.F., Back, L.H., "Flow and Heat Transfer Measurement in a Pseudo-Shock Region with Surface Cooling," *AIAA Journal* **14(12)**, 1716–1722, (1976).

[78] Inger, G.R., Lynch, F.T., Fancher, M.F., "Theoretical and experimental study of nonadiabatic transonic shock/boundary-layer interaction," *AIAA Journal* **23(10)**, 1476–1482, (1985).

[79] Castagna, A., "Experimental Research on the Transformation of Energy of a Gas Flowing in a Pipe," *Atti della Reale Accademia delle Scienze di Torino* **70**, 284–317, (1935).

[80] Tamaki, T., Tomita, T., Yamane, R., "Research on Pseudo-Shock (1st Report, -Type Pseudo-Shock)," *Bulletin of the JSME* **13(55)**, 191–226, (1970).

[81] Tamaki, T., Tomita, T., Yamane, R., "A Research on Pseudo-Shock (2nd Report, X-Type Pseudo-Shock)," *Bulletin of the JSME* **14(74)**, 807–817, (1971).

[82] Waltrup, P.J., Billig, F.S., "Structure of Shock Waves in Cylindrical Ducts," *AIAA Journal* **11(10)**, 1404–1408, (1973).

[83] Waltrup, P.J., Billig, F.S., "Prediction of Precombustion Wall Pressure Distributions in Scramjet Engines," *AIAA Journal of Spacecraft and Rockets* **10(9)**, 620–622, (1973).

[84] Waltrup, P.J., Cameron, J.M., "Wall Shear and Boundary-Layer Measurements in Shock Separated Flow," *AIAA Journal* **12(6)**, 878–880, (1974).

[85] Billig, F.S., "Research on Supersonic Combustion," *AIAA Aerospace Sciences Meeting, AIAA-92-0001, Reno, NV*, (1992).

[86] Wang, C.P., Zhang, K.Y., Cheng, K.M., "Pressure Distribution Measurements in Scramjet Isolators under Asymmetric Supersonic Flow," *44th AIAA Aerospace Science Meeting and Exhibit* **AIAA 2006-818**, (2006).

[87] Zimont, V.L., Ostras, V.N., "Calculation of pseudo-shocks in a cylindrical duct," *Fluid Mechanics Soviet Research*, **5(2)**, 78–87, (1976).

[88] Shchetinkov, E.S., "Piecewise-one-dimensional models of supersonic combustion and pseudo-shock in a duct," *Combustion, Explosion and Shock Waves*, **9(4)**, 409–417, (1973).

[89] Nagai, M., Yaga, M., "On the pseudo-shock wave relations," *In: Kral, L.D., Spina, E.F., Arakawa, C., Transitional and turbulent compressible flows, The American Society of Mechanical Engineers*, **224**, 103–108, (1995).

[90] Matsuo, K., Miyazato, Y., Kim, H.D., "Mass averaging pseudo-shock model in a straight flow passage," *Proceedings of the Institution of Mechanical Engineers* **213(6)**, 365–375, (1999).

[91] Ortwerth, P.J., "Scramjet Vehicle Integration," *In: Scramjet Propulsion, Progress in Astronautics and Aeronautics*, Washington DC, Chapter 17, (2001).

[92] Tu, Q., Segal, C., "Isolator/Combustion Chamber Interactions During Supersonic Combustion," *Journal of Propulsion and Power* **26(1)**, 182–186, (2010).

[93] Auslender, A.H., "An Analytic Performance Investigation of Mechanically Back- Pressured Ramjet Data," *JANNAF 34th*, October 27-31, (1997).

[94] Fischer, C., Olivier, H., "Experimental investigation of wall and total temperature influence on a shock train," *AIAA Journal* **52(4)**, 757–766, (2014).

[95] White, M.E., Drummond, J.P., Kumar, A., "Evolution and Application of CFD Techniques for Scramjet Engine Analysis," *Journal of Propulsion and Power* **3(5)**, 423–439, (1987).

[96] Mousavi, S.M., Roohi, E., "Three dimensional investigation of the shock train structure in a convergentdivergent nozzle," *Acta Astronautica* **105(1)**, 117–127, (2014).

[97] Baurle, R.A., Middleton, T.F., Wilson, L.G., "Reynolds-Averaged Turbulence Model Assessment for a Highly Back-Pressured Isolator Flowfield," *JANNAF 45th Combustion Meeting Joint Subcommittee Meeting, Monterey, CA*, (2012).

[98] Barber, T.J., Cox, G.B., "Hypersonic vehicle propulsion - A computational fluid dynamics application case study," *Journal of Propulsion and Power* **5(4)**, 492–501, (1989).

[99] Hunter, L.G., Couch, B.D., "A CFD Study of Precombustion Shock-Trains From Mach 3–6," *AIAA Paper No.90-2220*, (1990).

[100] Krishnan, L., Sandham, N.D., Steelant, J., "Shock-Wave/Boundary-Layer Interactions in a Model Scramjet Intake," *AIAA Journal* **47(7)**, 1680–1691, (2009).

[101] Nair, M.T., Naresh, K., Saxena, S.K., "Computational analysis of inlet aerodynamics for a hypersonic research vehicle," *Journal of Propulsion and Power* **21(2)**, 286–291, (2005).

[102] Mittal, S., Yadav, S., "Computation of flows in supersonic wind-tunnels," *Computer Methods in Applied Mechanics and Engineering*, **191(6–7)**, 611–634, (2001).

[103] Saha, S., Chakraborty, D., "Hypersonic intake starting characteristics-A CFD validation study," *Defence*

Science Journal **62(3)**, 147–152, (2012).

[104] Chan, W.Y.K., Jacobs, P.A., Mee, D.J., "Suitability of the $k-\varepsilon$ turbulence model for scramjet flowfield simulations," *International Journal for Numerical Methods in Fluids*, **70(4)**, 493–514, (2012).

[105] Acharya, M., Horstman, C.C., Kussoy, M.I., "Reynolds Number Effects on the Turbulence Field in Compressible Boundary Layers," *AIAA Journal* **17(4)**, 380–386, (1979).

[106] Atmani, R., Brima, A., Askovic, R., "Study of Three-Dimensional Separation of Boundary Layer over Blunt Bodies," *Journal of Hydrodynamics* **21(1)**, 100–107, (2009).

[107] Raghunathan, S., "Passive control of shock-boundary layer interaction," *Progress in Aerospace Sciences* **25(3)**, 271–296, (1988).

[108] Greene, B.R., Clemens, N.T., Micka, D.,"Control of shock boundary layer interaction using pulsed plasma jets," *51st AIAA Aerospace Sciences Meeting including the New Horizons Forum and Aerospace Exposition*, (2013).

[109] Im, S.K., Do, H., Godfrey Mungal, M., Cappelli, M.A., "Experimental study and plasma control of an unstarting supersonic flow," *6th AIAA Flow Control Conference 2012*, (2012).

[110] Stanewsky, E., Smith, G.E., "Adaptive wing and flow control technology," *Progress in Aerospace Sciences* **37(7)**, 583–667, (2001).

[111] Haack, S., Taylor, T., Cybyk, B., Foster, C., Alvi, F., "Experimental estimation of SparkJet efficiency," *AIAA Paper 2011-3997*, 971–983, (2011).

[112] Prandtl, L., "ber Flssigkeitsbewegung bei sehr kleiner Reibung," *In: Ludwig Prandtl Gesammelte Abhandlungen zur angewandten Mechanik, Hydro- und Aerodynamik*, 575–584, (1961).

[113] Ryu, K.J., Lim, S., Song, D.J., "A computational study of the effect of angles of attack on a double-cone type supersonic inlet with a bleeding system," *Computers & Fluids* **50(1)**, 72–80, (2011).

[114] Tindell, R. H., "Highly compact inlet diffuser technology," *Journal of Propulsion and Power* **4(6)**, 557–563, (1988).

[115] Kodera, M., Tomioka, S., Kanda, T., Mitani, T., Kobayashi, K., "Mach 6 test of a scramjet engine with boundary-layer bleeding and two-staged fuel injection," *AIAA-2003-7049*, (2003).

[116] Weise, A., "The separation of flow due to compressibility shock," *NACA Technical Memorandum* **No.1152**, (1947).

[117] Anderson, J.D.J., "Airframe/Propulsion Integration of Supersonic Vehicles," *26th AIAA/SAE/ASME/ASEE Joint Proportion Conference, AIAA 90-2151, Orlando, Fl*, (1990).

[118] Harloff, G.J., Smith, G.E., "Supersonic-inlet boundary-layer bleed flow," *AIAA Journal* **34(4)**, 778–

785, (1996).

[119] Schulte, D., Henckels, A., Schell, I., "Boundary Layer Bleed in Hypersonic Inlets," *New Results in Numerical and Experimental Fluid Mechanics - Contributions to the 10th AG STAB/DGLR Symposium Braunschweig, Germany 1996* **60**, 296–303, (1997).

[120] Kornilov, V.I., "Current state and prospects of researches on the control of turbulent boundary layer by air blowing," *Progress in Aerospace Sciences* **76**, 1–23, (2015).

[121] Paynter, G.C., Treiber, D.A., Kneeling, W.D., "Modeling supersonic inlet boundary-layer bleed roughness," *Journal of Propulsion and Power* **9(4)**, 622–627, (1993).

[122] Syberg, J., Hickcox, T.E., "Design of a bleed system for a Mach 3.5 inlet," *NASA CR-2187*, (1973).

[123] Cebeci, T., Chang, K.C., "Calculation of incompressible rough-wall boundary-layer flows," *AIAA Journal* **16(7)**, 730–735, (1978).

[124] Bowditch, D.N., "Some design considerations for supersonic cruise mixed compression inlets," *NASA TM X-71460*, (1973).

[125] Loth, E., "Smart mesoflaps for control of shock boundary layer interactions," *AIAA Paper 2000-2476*, (2000).

[126] Gefroh, D., Loth, E., Dutton, C., Hafenrichter, E., "Aeroelastically deflecting flaps for shock/boundary-layer interaction control," *Journal of Fluids and Structures* **17(7)**, 1001–1016, (2003).

[127] McCormick, D.C., "Shock/boundary-layer interaction control with vortex generators and passive cavity," *AIAA Journal* **31(1)**, 91–96, (1993).

[128] Smith, A.N., Babinsky, H., Fulker, J., Ashill, P.R., "Shockwave/boundary-layer interaction control using streamwise slots in transonic flows," *Journal of Aircraft* **41(3)**, 540–546, (2004).

[129] Srinivasan, K.R., Loth, E., Dutton, C.J., "Aerodynamics of Recirculating Flow Control Devices for Normal Shock/Boundary-Layer Interactions," *AIAA Journal* **44(4)**, 751–763, (2006).

[130] Hafenrichter, E., Lee, Y., Dutton, J., Loth, E., "Normal Shock/Boundary-Layer Interaction Control Using Aeroelastic Mesoflaps," *Journal of Propulsion and Power* **19(3)**, 464–472, (2003).

[131] Holden, H., Babinsky, H., "Effect of microvortex generators on separated normal shock/boundary layer interactions," *Journal of Aircraft* **44(1)**, 170–174, (2007).

[132] Hadjadj, A., Dussauge, J.P., "Shock wave boundary layer interaction," *Shock Waves* **19**, 449–452, (2009).

[133] Babinsky, H., Li, Y., Ford, C.W.P., "Microramp Control of Supersonic Oblique Shock-Wave/Boundary-Layer Interactions," *AIAA Journal* **47(3)**, 668–675, (2009).

[134] Saad, M.R., Zare-Behtash, H., Che Idris, A., Kontis, K., "Micro-ramps for hypersonic flow control," *Micromachines* **3**, 364–378, (2012).

[135] Caraballo, E., Webb, N., Little, J., Kim, J.H., Samimy, M., "Supersonic Inlet Flow Control Using Plasma Actuators," *AIAA Paper 2009-0724*, (2009).

[136] Ogawa, H., Babinsky, H., Ptzold, M., Lutz, T.,"'Shock-Wave/Boundary-Layer Interaction Control Using Three-Dimensional Bumps for Transonic Wings," *AIAA Journal* **46(6)**, 1442–1452, (2008).

[137] Ashill, P.R., Fulkner, J.L., Shires, A., "A Novel Technique for Controlling Shock Strength of Laminar-Flow Aerofoil Sections," *Proceedings 1st European Forum on Laminar Flow Technology, Hamburg*, 175-183, (1992).

[138] Bruce, P.J.K., Babinsky, H., "Experimental Study into the Flow Physics of Three-Dimensional Shock Control Bumps," *Journal of Aircraft* **49(5)**, 1222–1233, (2012).

[139] Lim, S., Kim, S.D., Song, D.J., "A computational study on the efficiency of boundary layer bleeding for the supersonic bump type inlet," *47th Aerospace sciences meeting*, 5–8, (2009).

[140] Ogawa, H., Babinsky, H., "Shock/boundary-layer interaction control using three-dimensional bumps in supersonic engine inlets," *46th AIAA Aerospace Sciences Meeting and Exhibit, Reno, NV*, (2008).

[141] Zhang, Y., Tan, H.J., Tian,F.C., Zhuang, Y., "Control of Incident Shock/Boundary-Layer Interaction by a Two-Dimensional Bump," *AIAA Journal* **52(4)**, 767–776, (2014).

[142] Leconte, J., "On the Influence of Musical Sounds on the Flame of a Jet of Coal-Gas," *Philosophical Magazine* **15**, 235–239, (1858).

[143] Qin, B., Chang, J., Jiao, X., Bao, W., Yu, Y., "Numerical investigation of the impact of asymmetric fuel injection on shock train characteristics," *Acta Astronautica* **105(1)**, 66–74, (2014).

[144] Sahoo, D., Annaswamy, A.M., Alvi, F., "Active Store Trajectory Control in Supersonic Cavities Using Microjets and Low-Order Modeling," *AIAA Journal* **45(3)**, 516–531, (2007).

[145] Kumar, V., Farrukh, A., "Efficient Control of Separation using Microjets," *AIAA Paper 2005-4879*, (2005).

[146] Ali, M.Y., Solomon, J.T., Gustavsson, J., Kumar, R., Alvi, F.S., "Control of Resonant Flow Inside a Supersonic Cavity Using High Bandwidth Micro-Actuators," *AIAA Paper 2010-1198*, (2010).

[147] Samimy, M., Kearney-Fisher, M., Kim, J., Sinha, A., "High speed and High Reynolds Number Jet Control Using Arc Filament Plasma Actuators for Noise Mitigation and for Flow and Noise Diagnostics," *J49th Aerospace Sciences Meeting, Orlando, FL*, (2011).

[148] Ukai, T., Zare-Behtash, H., Erdem, E., Kin Hing, L., Kontis, K., Obayashi, S., "Effectiveness of jet

location on mixing characteristics inside a cavity in supersonic flow," *Experimental Thermal and Fluid Science* **52**, 59–67, (2014).

[149] Ukai, T., Zare-Behtash, H., Kin Hing, L., Kontis, K., Obayashi, S., "Effects of dual jets distance on mixing characteristics and flow path within a cavity in supersonic crossflow," *International Journal of Heat and Fluid Flow* **50**, 254–262, (2014).

[150] Zare-Behtash, H., Kin Hing, L., Kontis, K., Ukai, T., Obayashi, S., "Transverse jet-cavity interactions with the influence of an impinging shock," *International Journal of Heat and Fluid Flow* **53**, 146–155, (2015).

[151] Utkin, Y.G., Keshav, S., Kim, J.H., Kastner, J., Adamovich, I.V., Samimy, M., "Development and use of localized arc filament plasma actuators for high-speed flow control," *Journal of Physics D Applied Physics* **40(3)**, 685–694, (2003).

[152] Samimy, M., Kim, J.H., Kastner, J., Adamovich, I., Utkin, Y., "Active control of high-speed and high-Reynolds-number jets using plasma actuators," *Journal of Fluid Mechanics* **578**, 305–330, (2007).

[153] Kalra, C.S., Zaidi, S., Miles, R.B., "Shockwave Induced Turbulent Boundary Layer Separation Control with Plasma Actuators," *Published in: 46th AIAA Aerospace Sciences Meeting and Exhibit*, (2008).

[154] MacHeret, S.O., Shneider, M.N., Miles, R.B., "Magnetohydrodynamic Control of Hypersonic Flows and Scramjet Inlets Using Electron Beam Ionization," *AIAA Journal* **40(1)**, 74–81, (2002).

[155] Roupassov, D.V., Nikipelov, A.A., Nudnova, M.M., Starikovskii, A.Y., "Flow Separation Control by Plasma Actuator with Nanosecond Pulsed-Periodic Discharge," *AIAA Journal* **47(1)**, 168–185, (2009).

[156] Adelgren, R.G., Elliott, G.S., Crawford, J.B., Carter, C.D., Donbar, J.M., Grosjean, D.F., "Axisymmetric Jet Shear-Layer Excitation Induced by Laser Energy and Electric Arc Discharges," *AIAA Journal* **43(4)**, 776–791, (2005).

[157] Grossman, K.R., Cybyk, B.Z., Rigling, M.C., VanWie, D.M., "Characterization of sparkjet actuators for flow control," *42nd AIAA Aerospace Sciences Meeting and Exhibit, Reno, NV*, 3957–3964, (2004).

[158] Narayanaswamy, V., Raja, L.L., Clemens, N.T., "Control of a shock/boundary-layer interaction by using a pulsed-plasma jet actuator," *AIAA Journal* **50(1)**, 246–249, (2012).

[159] Opaits, D.F., Roupassov, D.V., Saddoughi, S.G., Starikovskaia, S.M., Zavialov, I.N., Starikovskii, A.Y., "Plasma Control of Boundary Layer Using Low-Temperature Non-Equilibrium Plasma of Gas Discharge," *AIAA Paper 2005-1180*, (2005).

[160] Velkoff, H., Ketchman, J., "Effect of an Electrostatic Field on Boundary Layer Transition," *AIAA Journal* **6(7)**, 1381–1383, (1968).

[161] Léger, L., Moreau, E., Artana, G., Touchard, G., "Influence of a DC corona discharge on the airflow along an inclined flat plate," *Journal of Electrostatics* **50–51**, 300–306, (2001).

[162] Tan, H.J., Li, C.H., Zhang, Y., "Investigation of a Fluidic Shock Control Method for Hypersonic Inlets," *Journal of Propulsion and Power* **26(5)**, 1072–1083, (2010).

[163] Hutzel, J.R., Decker, D.D., Cobb, R.G., King, P.I., Veth, M.J., "Scramjet isolator shock train location techniques," *49th AIAA Aerospace Sciences Meeting including the New Horizons Forum and Aerospace Exposition, Orlando, Florida*, (2011).

[164] Le, D.B., Goyne, C.P., Krauss, R.H., "Shock Train Leading-edge detection in a dual-mode scramjet," *Journal of Propulsion and Power* **24(5)**, 1035–1041, (2008).

[165] Chang, J., Li, B., Bao, W., Yu, D., "Shock train leading-edge detection in an isolator using genetic algorithm," *Proceedings of the Institution of Mechanical Engineers, Part G. Journal of Aerospace Engineering* **226(11)**, 1424–1431, (2012).

Figure 1. The experimental ramjet aircraft Leduc 0.10[5]

Figure 2. The Nord 1500 Griffon in 1955[5]

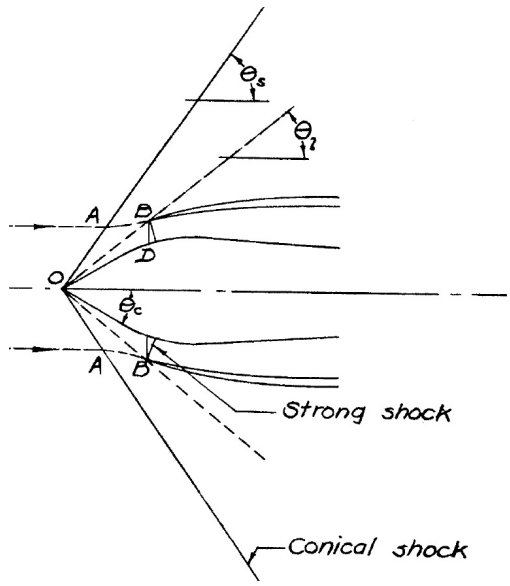

Figure 3. Schematic of the fixed geometry inlet proposed by Ferri[8]

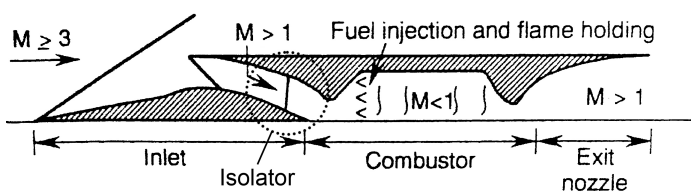

Figure 4. Schematic of a conventional ramjet engine[10]

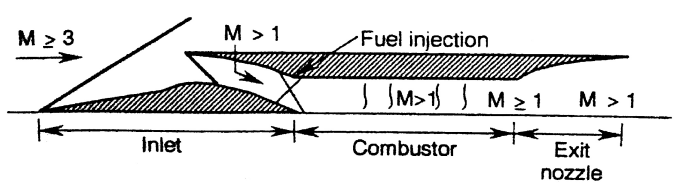

Figure 5. Schematic of a scramjet engine[10]

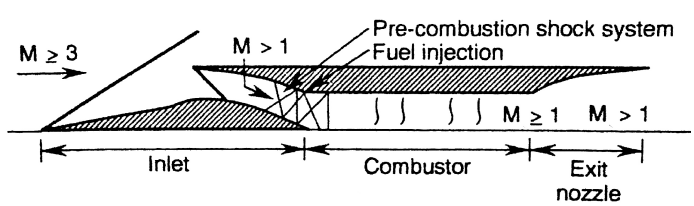

Figure 6. Schematic of a dual-mode ram-scramjet engine[10]

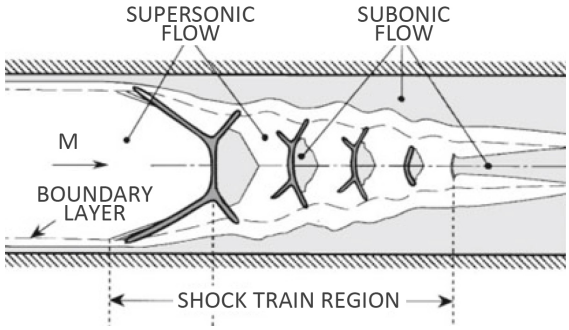

Figure 7. Two-dimensional sketch of the shock wave/boundary layer interaction[27]

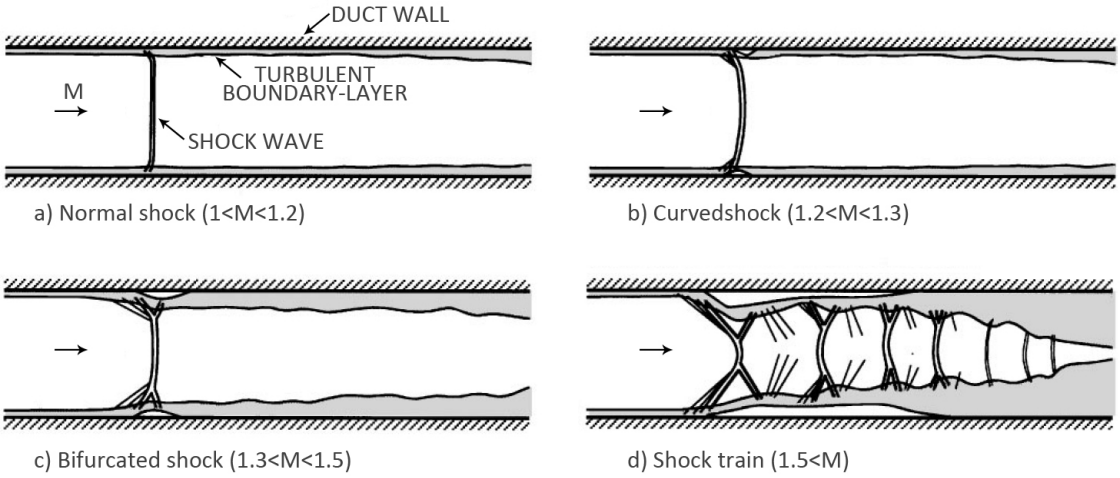

Figure 8. Schematic of shock wave/boundary layer interaction in a constant area duct[24]

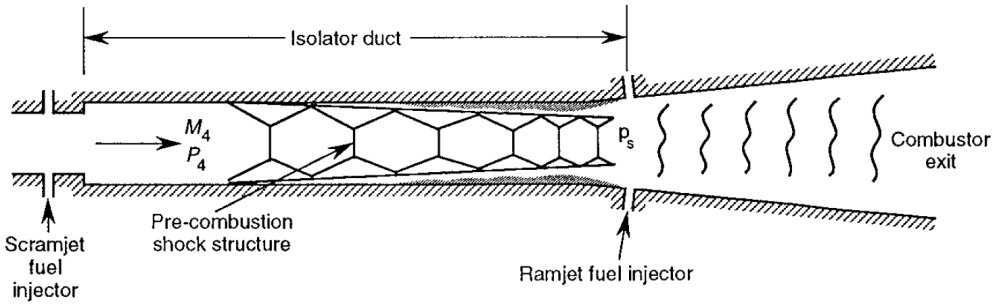

Figure 9. Schematic of a scramjet combustor utilised as an isolator duct in the ramjet mode of operation[13]

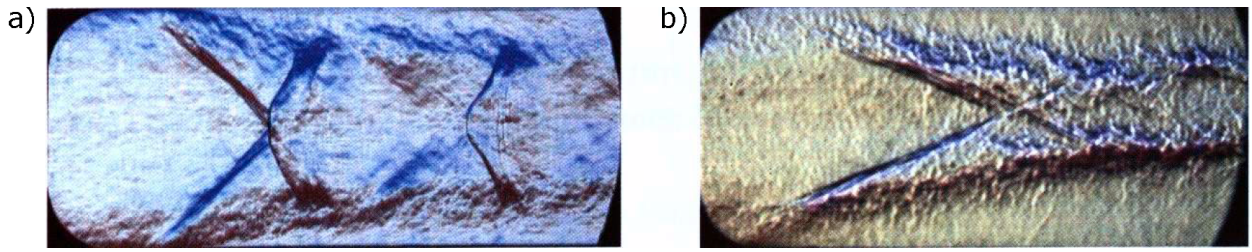

Figure 10. Schlieren photographs of: a) λ shock train at M=2; b) χ shock train at M=4[40]

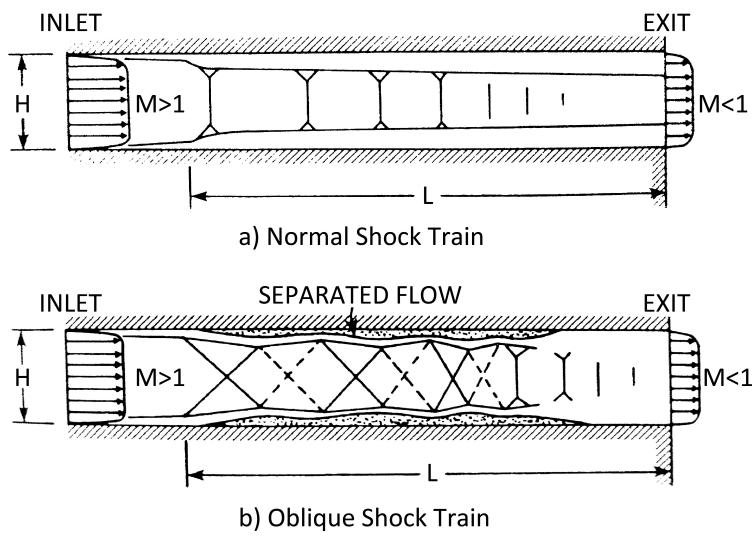

Figure 11. Schematic of the flow pattern of a: a) normal shock train; b) oblique shock train[41]

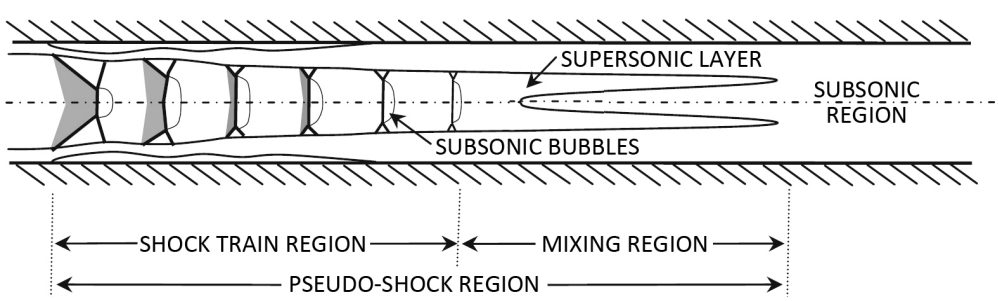

Figure 12. Sketch of a pseudo-shock system (Weiss et al.[31])

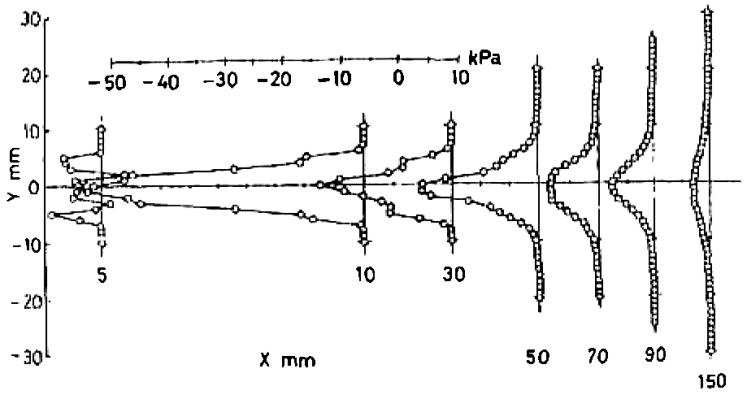

Figure 13. Radial distribution of static pressure across the shock train system (Nagai[44])

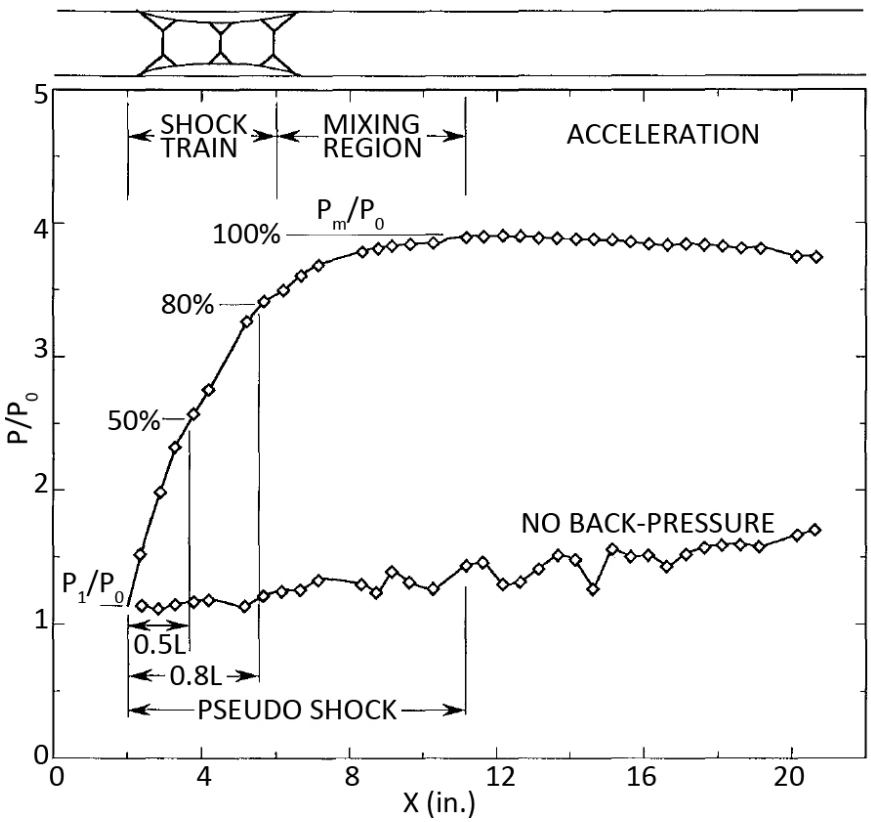

Figure 14. Pressure variation through the shock train at Mach number of 2[13]

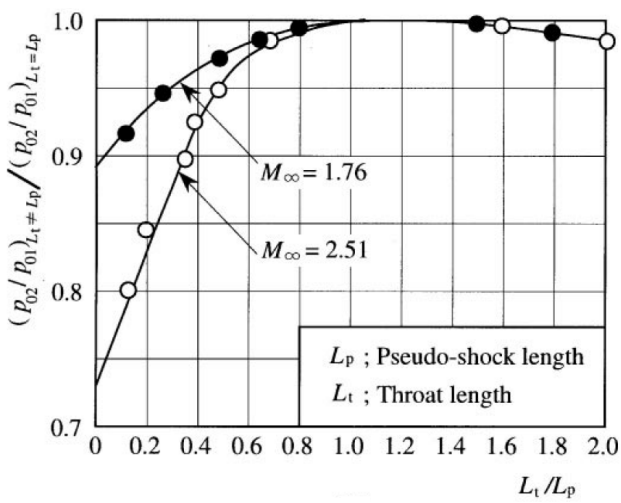

Figure 15. Total pressure recovery as a function of isolator and pseudo-shock lengths[48]

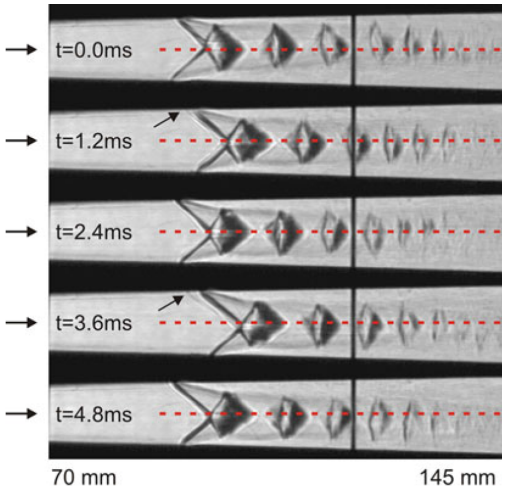

Figure 16. Schlieren image of the oscillating and asymmetric pseudo-shock system[27]

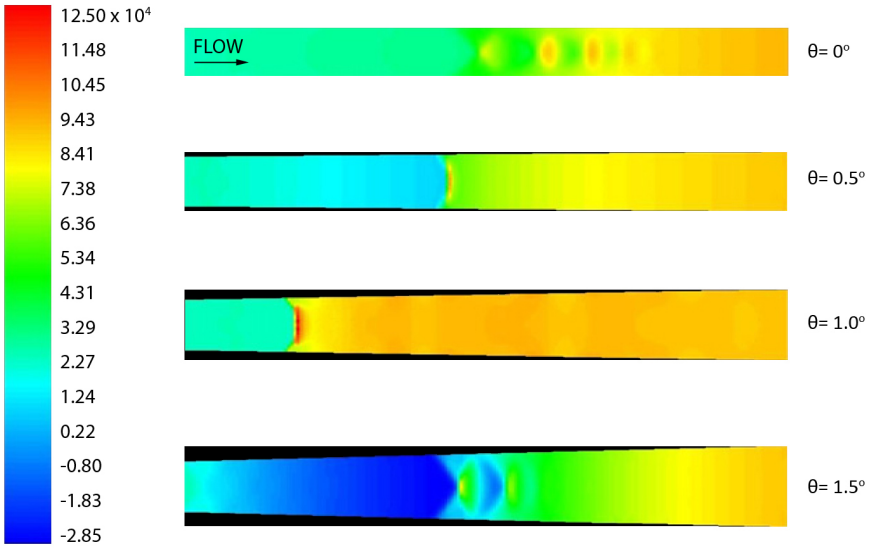

Figure 17. Numerical static pressure contours in Mach 2 scramjet isolators with different divergence angles[21]

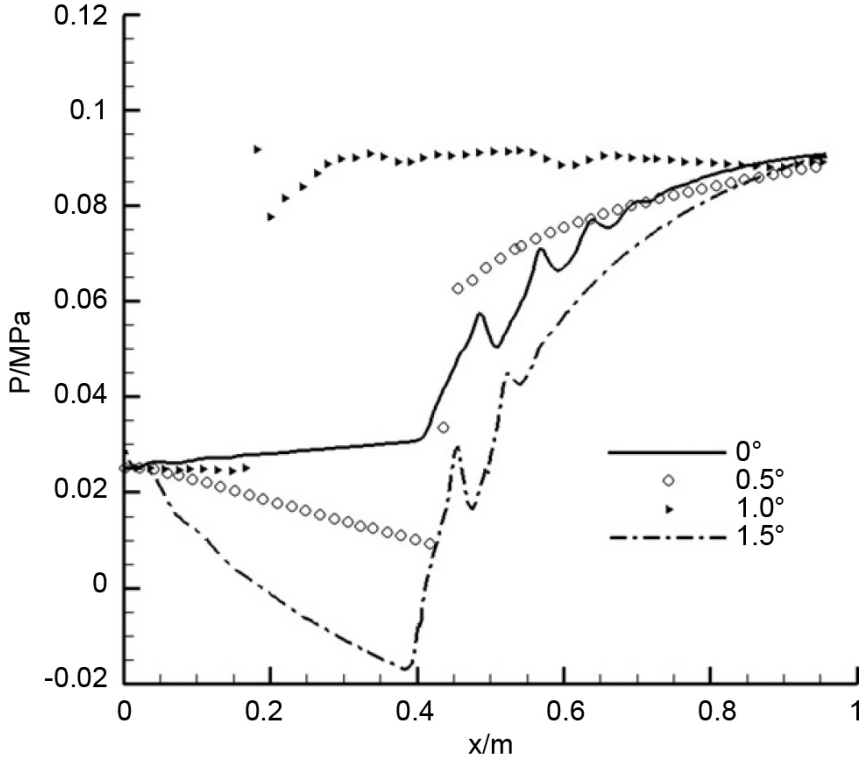

Figure 18. Static pressure distribution along the centreline of the duct in Mach 2 scramjet isolators with different divergent angles and constant back-pressure of 90 kPa[21]

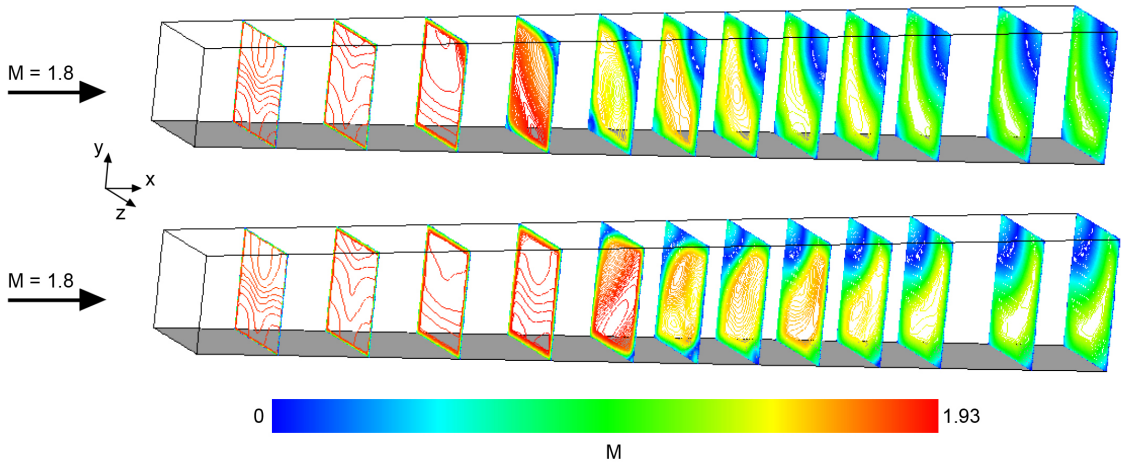

Figure 19. Numerical Mach number contours in diverging duct atflow mach number of 1.8[67]

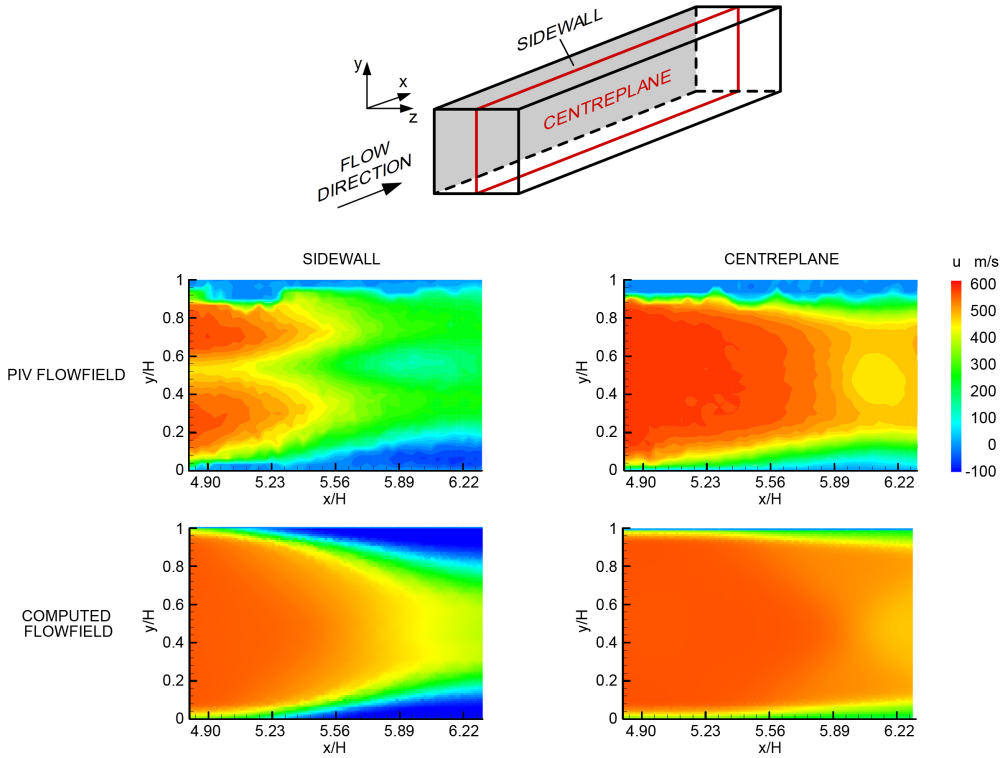

Figure 20. Contours of the streawise component of the velocity vector on x-y plane in a constant area duct at flow Mach number of 2.3[67]

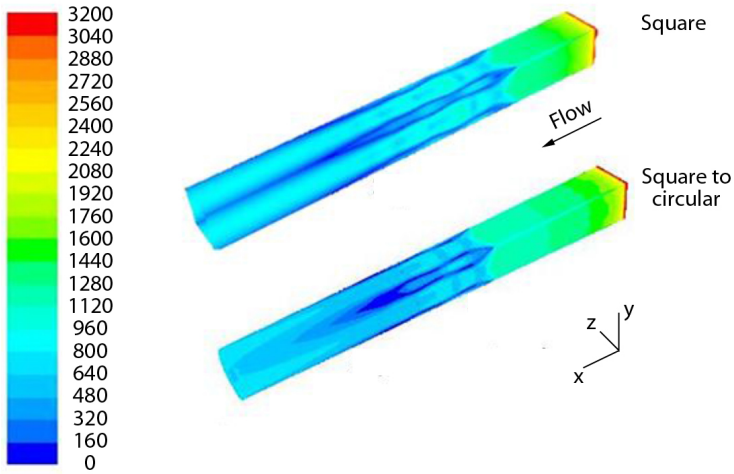

Figure 21. Wall shear stress contour in a square duct and a square-to-circular isolators[75]

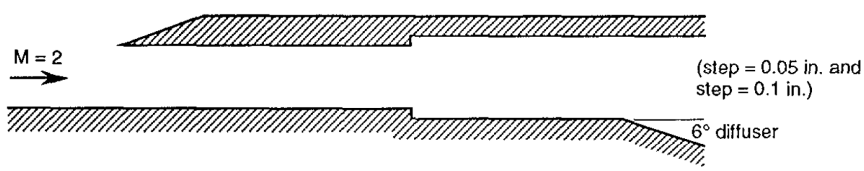

Figure 22. Schematic of a rectangular isolator with a step[13]

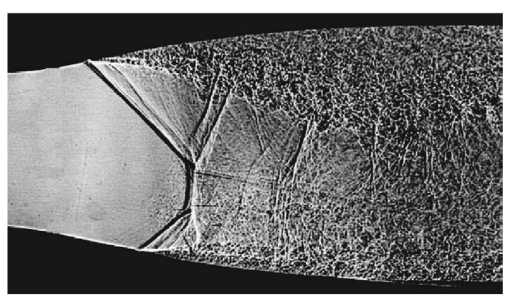

Figure 23. Non-symmetrical pseudo-shock in a planar supersonic nozzle[30]

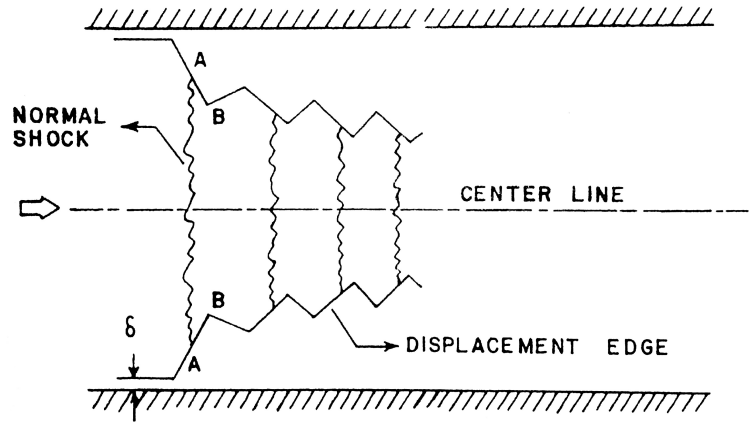

Figure 24. One-dimensional flow model of the formation of multiple shock waves in a duct[26]

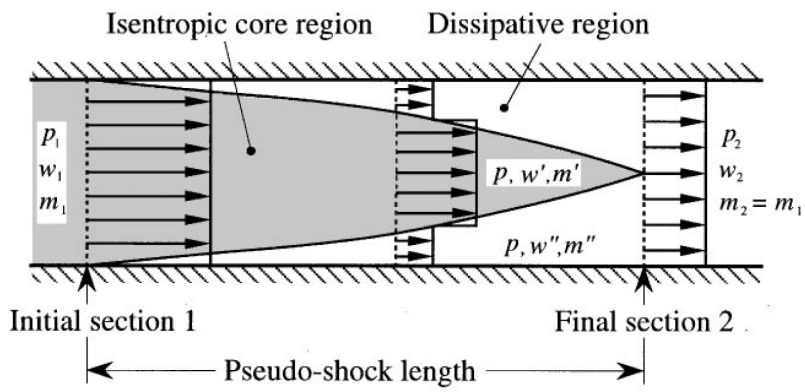

Figure 25. Crocco's shockless model[23]

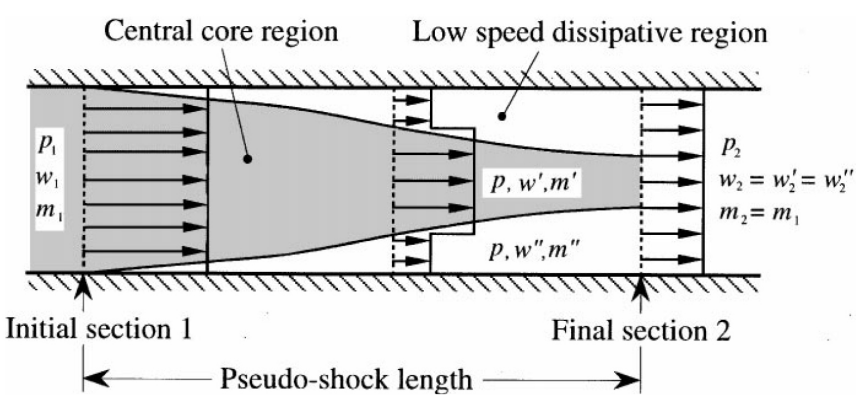

Figure 26. Diffusion model proposed by Ikui et al.[35]

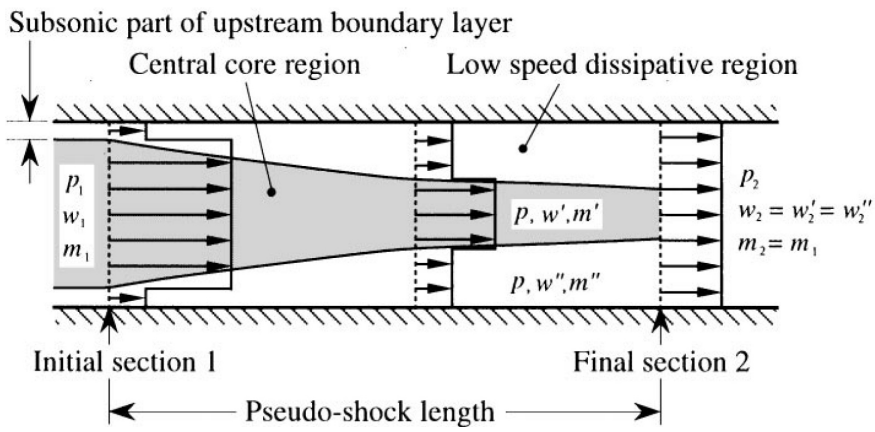

Figure 27. Modified diffusion model[46]

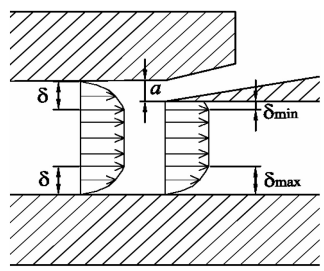

Figure 28. Boundary layer asymmetry at the isolator entrance[86]

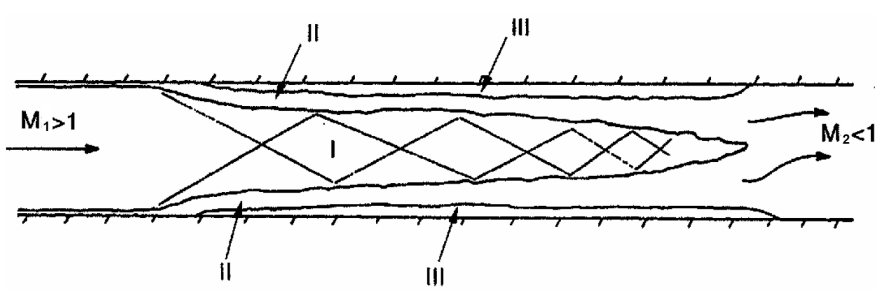

Figure 29. Flow model for separation in a duct developed by Ortwerth[91]

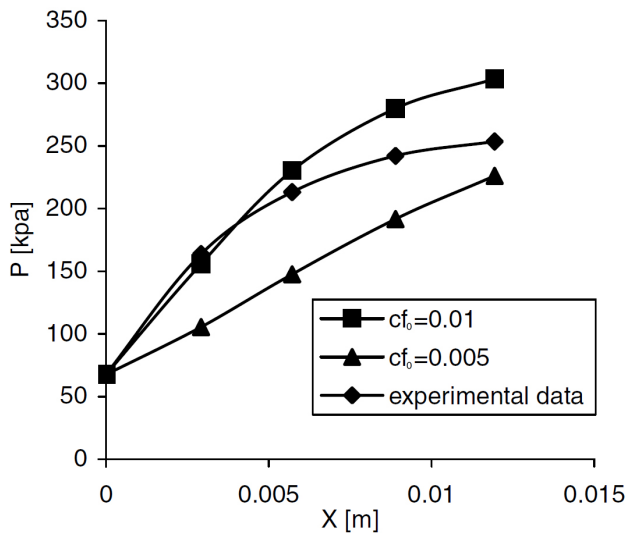

Figure 30. Influence of the wall friction coefficient on the isolator pressure rise[92]

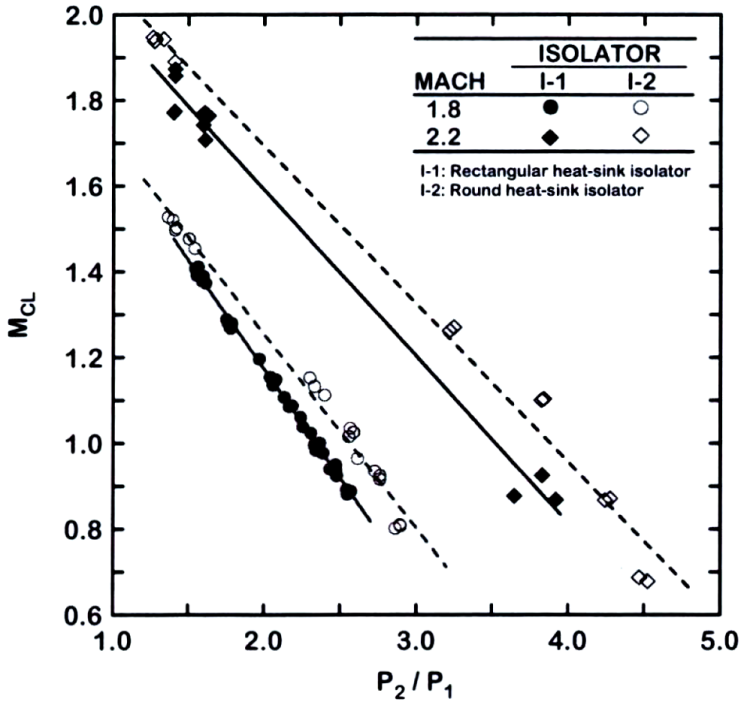

Figure 31. Relationship between the centreline Mach number M_{CL} at the isolator exit with the pressure ratio P_2/P_1[74]

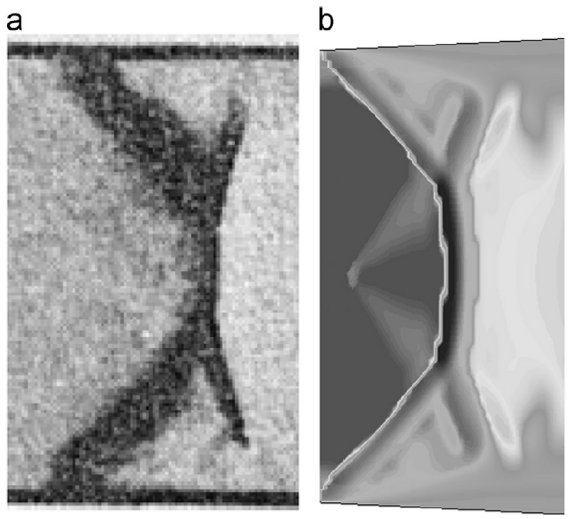

Figure 32. Comparison of λ shock a) Experimental; b) Numerical[96]

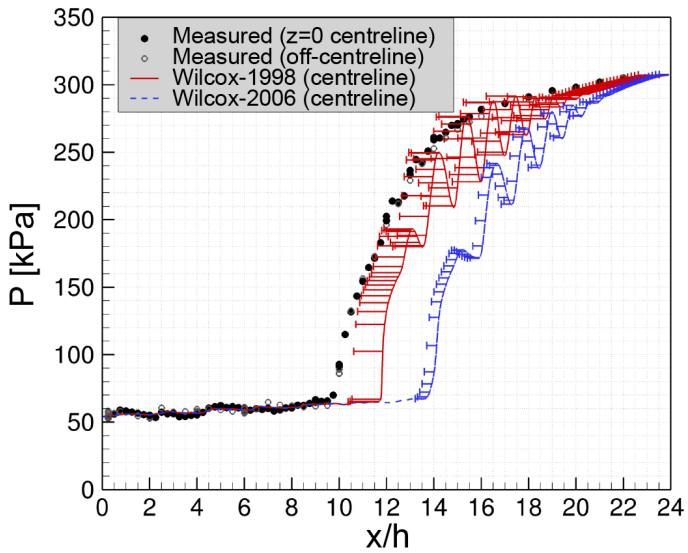

Figure 33. Comparison of wall pressure measurement with computed results[97]

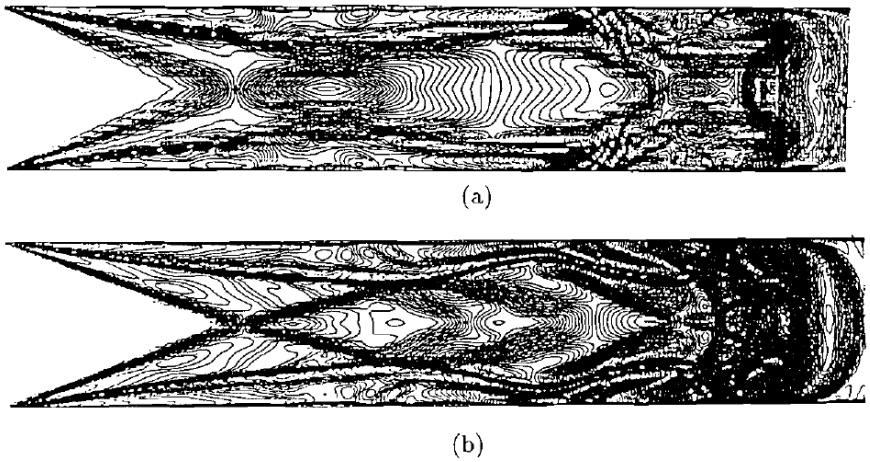

Figure 34. Density contours at $M = 3$. a) 350×77 grid points; b) 350×153 grid points[39]

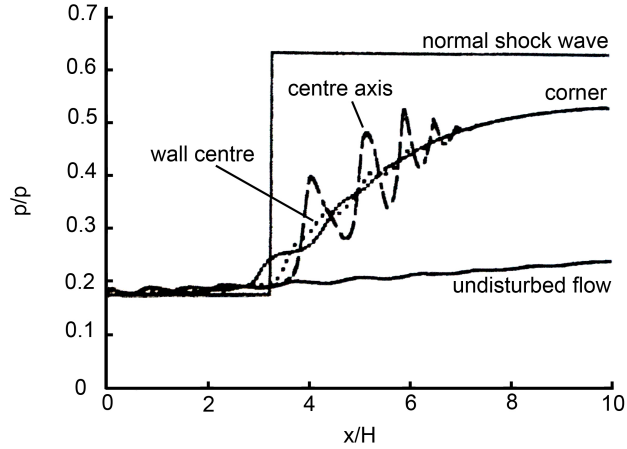

Figure 35. Static pressure distribution in a constant area duct at Mach 1.8[67]

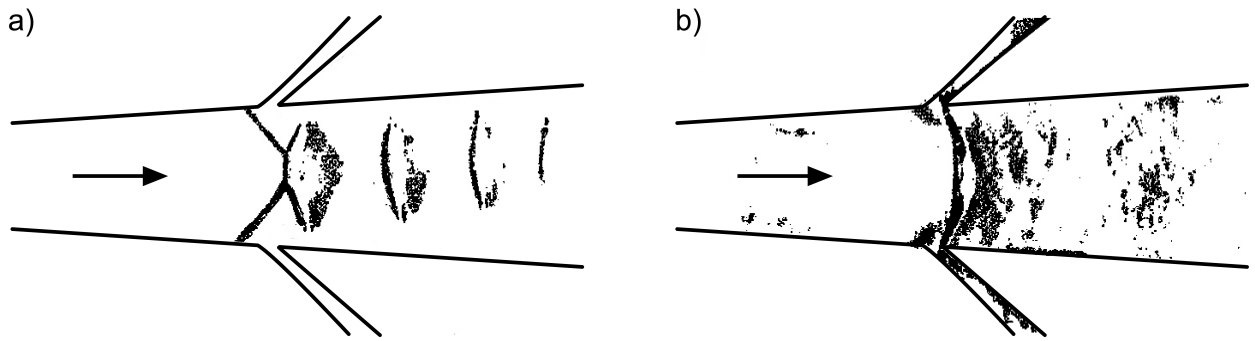

Figure 36. Boundary-layer control in diverging channel. a) No control; b) Boundary-layer suction[116]

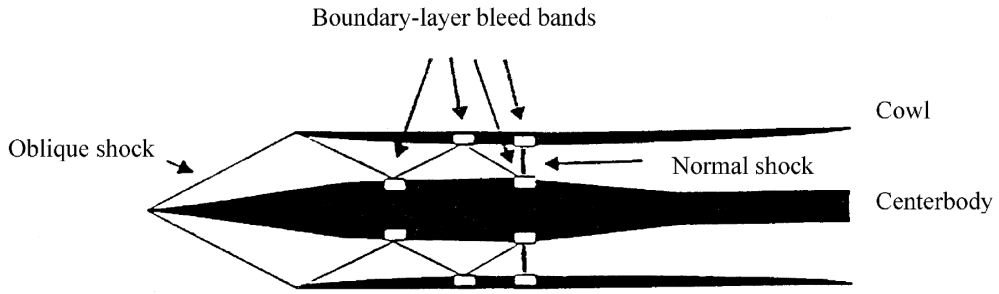

Figure 37. Boundary-layer bleed in a mixed-compression supersonic inlet[126]

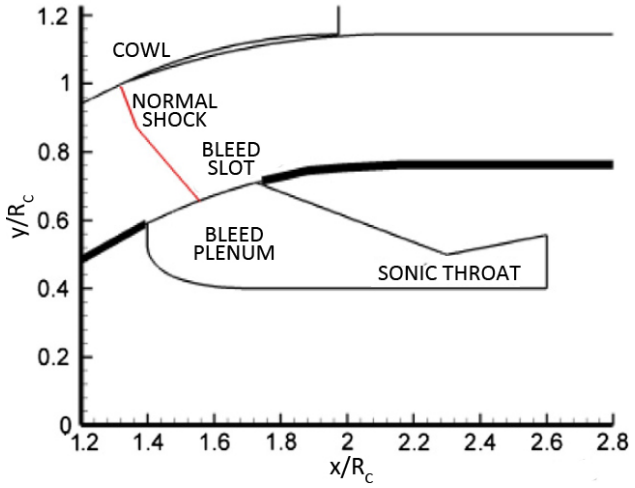

Figure 38. Schematic of a bleeding-system geometry[139]

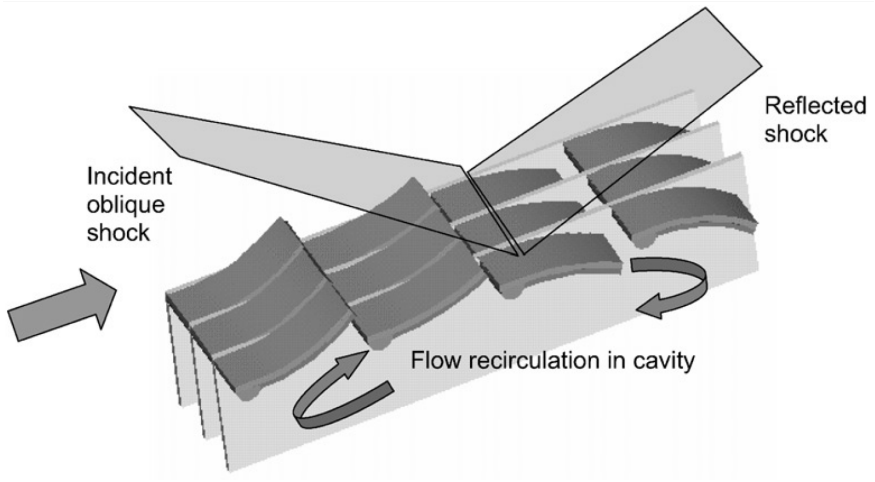

Figure 39. Schematic of aeroelastic mesoflaps[126]

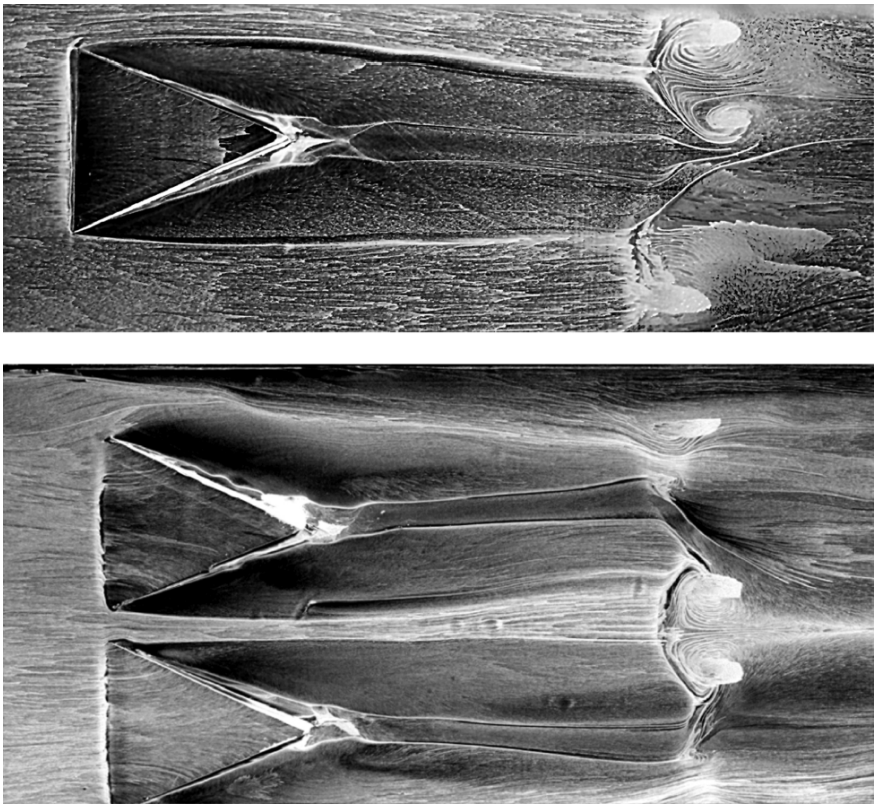

Figure 40. Microramp flow visualisation in single and array configuration[133]

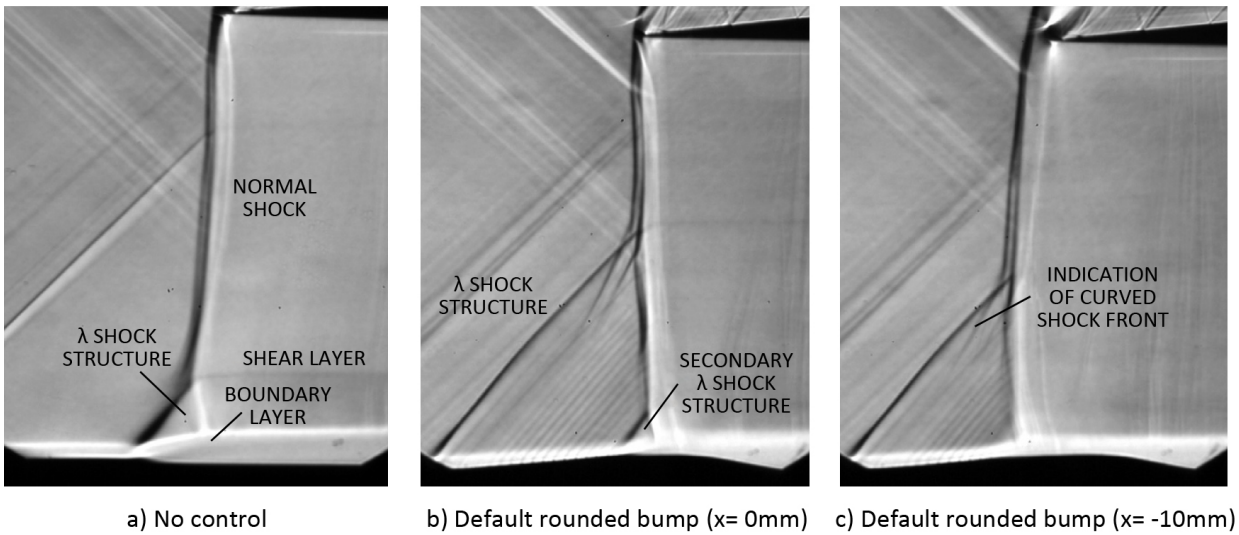

Figure 41. Effect of two-dimensional bumps on shock wave/boundary-layer interactions[140]

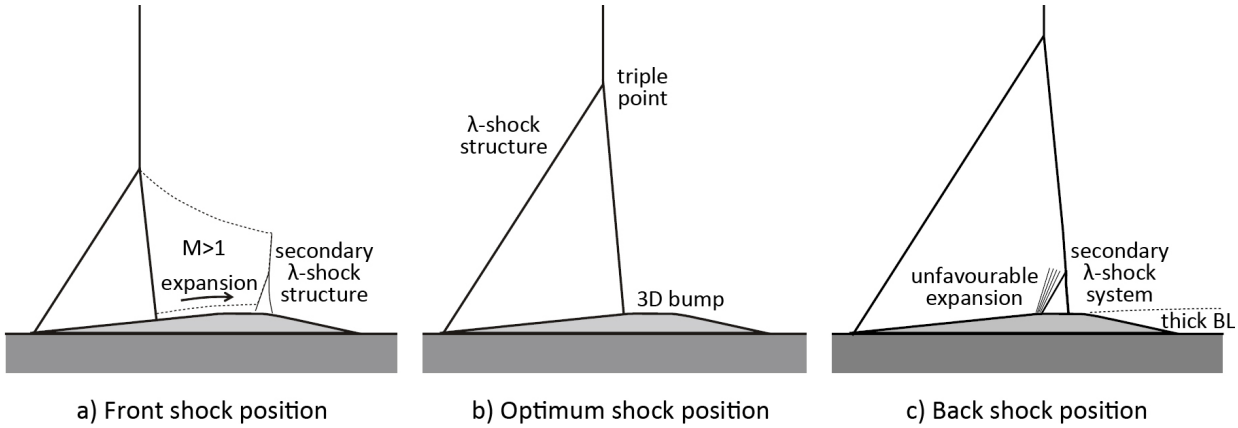

Figure 42. Schematic of λ shock configuration at various shock positions[140]

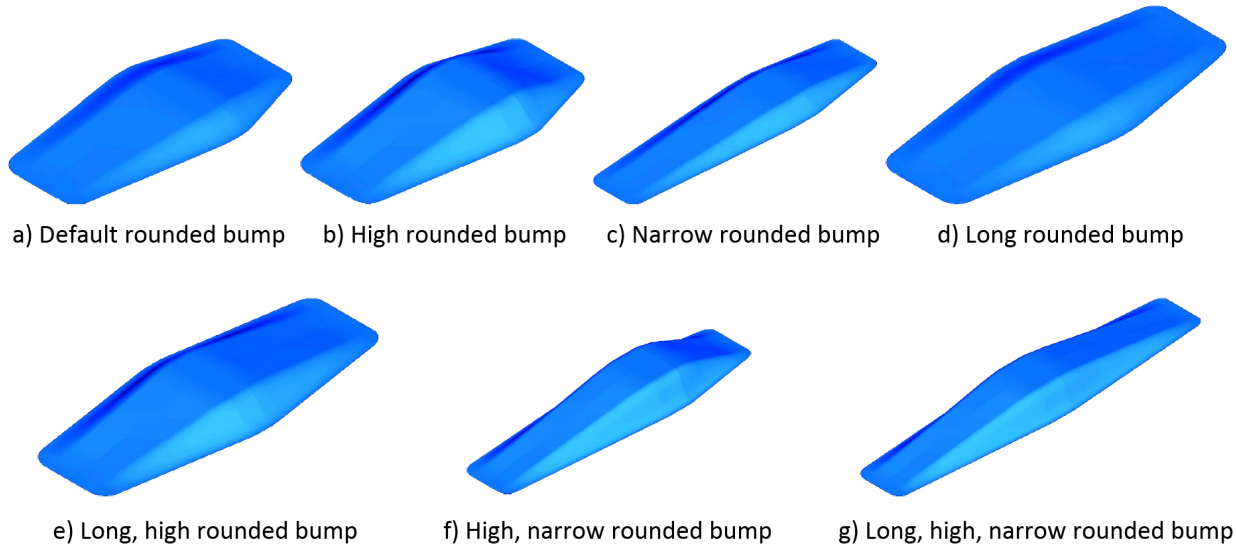

Figure 43. Schematic of different three-dimensional bumps[140]

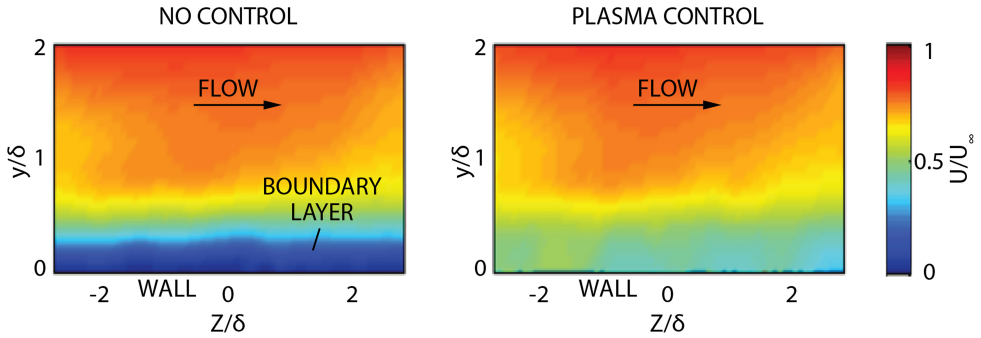

Figure 44. PIV streamwise velocity map in a Mach 2 inlet flow[135]